



Cite this: *RSC Appl. Polym.*, 2023, **1**, 158

# Thermoresponsive polymers with LCST transition: synthesis, characterization, and their impact on biomedical frontiers

Yichun Yuan,<sup>a</sup> Konpal Raheja,<sup>a</sup> Nathalie B. Milbrandt,<sup>a</sup> Sophia Beilharz,<sup>†a</sup> Steffy Tene,<sup>a</sup> Solomon Oshabaheebwa,<sup>b</sup> Umut A. Gurkan,<sup>b,c</sup> Anna Cristina S. Samia<sup>a</sup> and Metin Karayilan<sup>a</sup>

Advances in thermoresponsive materials have significantly impacted many biomedical fields. The unique behavior of reversible phase transition close to the physiological temperatures makes these types of materials a great candidate for a wide variety of biomedical applications including bioimaging, biosensing, injectables, smart surfaces, adhesives, biomanufacturing, and tissue engineering. Thermoresponsive behavior, mainly lower critical solution temperature (LCST) can be easily tuned by shifting the balance between hydrophobicity and hydrophilicity (e.g., by using comonomers or changing end groups) and modifying the molecular weight and architecture of the polymer. Hence, synthetic and characterization tools are critical in tailoring and precisely determining these properties. This review aims to show the full scope of the journey of thermoresponsive polymers from benchtop to potential applications. We especially intend to emphasize the effects of the structural heterogeneity of polymers on thermal transition and highlight the modern characterization techniques used to study thermoresponsive behavior. A better understanding of these structural effects and benchtop tools can help us design and implement more advanced materials for future applications in public health.

Received 15th July 2023,  
Accepted 24th August 2023

DOI: 10.1039/d3lp00114h

rsc.li/rscapppolym

## 1. Introduction

Polymers can be engineered to exhibit responses to a diverse variety of external stimuli including changes in temperature,<sup>1–5</sup> light,<sup>6–9</sup> pH,<sup>10–12</sup> magnetic fields,<sup>13–16</sup> electric fields,<sup>17–19</sup> ultrasonication,<sup>20,21</sup> mechanical forces,<sup>22,23</sup> and many others.<sup>24–28</sup> Arguably, thermoresponsive behavior of polymers is studied most extensively in these stimuli-responsive materials space. The earliest works on thermoresponsive properties of poly(*N*-isopropylacrylamide) (PNIPAM) were documented in the late 1960s.<sup>29,30</sup>

Thermoresponsive polymers can undergo reversible phase transition upon exposure to temperature change. Polymers that show a lower critical solution temperature (LCST) behavior in an aqueous solution are soluble below LCST due to extensive hydrogen bonding interactions between the

polymer and surrounding water molecules. Above LCST, hydrogen bonding with water molecules is disturbed and the intra- and intermolecular hydrophobic and hydrogen bonding interactions become more dominant, as a result, the polymer becomes insoluble in an aqueous solution upon heating.<sup>31</sup> When water molecules are repelled from the polymer chain at elevated temperatures, hydrogen bonds (between water and polymer chain) are broken and new hydrogen bonds are formed resulting in a change in enthalpy. In addition, entropy increases as water molecules are no longer constrained. Hence, based on Gibbs free energy equation ( $\Delta G = \Delta H - T\Delta S$ ), phase transition from soluble to insoluble polymer chains becomes spontaneous as the temperature gets above the threshold value (LCST) due to so-called “hydrophobic effect”.<sup>32,33</sup> PNIPAM chains, for example, are soluble in water below its LCST due to the interactions between amide groups on side chains and water molecules, forming solvated random coils. At elevated temperatures, side chains favorably interact with each other resulting in the transformation from soluble coils to insoluble globules. The temperature of the coil-to-globule transition is called the cloud point temperature ( $T_{cp}$ ) at which a phase transition occurs from fully transparent to opaque solution (generally at

<sup>a</sup>Department of Chemistry, Case Western Reserve University (CWRU), Cleveland, Ohio 44106, USA. E-mail: metin.karayilan@case.edu

<sup>b</sup>Department of Biomedical Engineering, CWRU, Cleveland, Ohio 44106, USA

<sup>c</sup>Department of Mechanical and Aerospace Engineering, Case Comprehensive Cancer Center, CWRU, Cleveland, Ohio 44106, USA

<sup>†</sup>These authors contributed to writing the original draft equally.





**Fig. 1** Schematic representation of (A) a polymer phase transition of PNIPAM in aqueous solution from a completely dissolved homogeneous state (left, solvated random coil) to a two-phase demixed system (right, insoluble globule) and (B) the coil-to-globule transition with polymer solvation through hydrogen bonding below the LCST and domination of the hydrophobic interactions above the LCST. Adapted with permission from ref. 34 and 40. Copyright 2022, RSC and 2020, Elsevier.

50% transmittance) due to the formation of stable polymer agglomerates with a size larger than visible light (Fig. 1).<sup>34</sup> The LCST is defined as the minimum value of the  $T_{cp}$  in the temperature–concentration phase diagram.<sup>35</sup> The LCST behavior of polymers in an aqueous solution can be tuned by chemically incorporating hydrophilic or hydrophobic character to the original polymer through copolymerization and end group transformation/functionalization, modifying the polymer architecture and molecular mass (*e.g.*, weight average molecular weight,  $M_w$  or number average molecular weight,  $M_n$ ), and adjusting ionic strength (*e.g.*, salt type or concentration). The tunability of LCST makes the thermoresponsive polymers ideal for use in physiological temperatures, typically 35–40 °C range.<sup>36–39</sup>

These polymers have gained significant attention in recent years<sup>41–49</sup> due to their potential applications in several biomedical fields such as bioimaging,<sup>50</sup> drug delivery,<sup>51–56</sup> injectables,<sup>57–63</sup> smart surfaces,<sup>64–75</sup> adhesives,<sup>76</sup> and tissue engineering.<sup>77–80</sup> However, the effects of the structural heterogeneity of polymers on thermal transition and modern characterization techniques have not been systematically discussed before. The precise determination of phase transition and LCSTs of these novel materials play a critical role in biomedical applications, where tolerance for error is generally infinitesimal. In this review, we aim to show the full scope of the journey of thermoresponsive polymers from their synthesis to biomedical frontiers. This review article (1) highlights the most common thermoresponsive polymers such as poly(*N*-alkyl acrylamide) and polyethylene glycol (PEG) derivatives; (2) provides a brief summary of controlled radical polymerization (CRP) techniques for synthesis and structural property control of thermoresponsive polymers; (3) discusses the effects of structural heterogeneity (*e.g.*, architecture, molecular mass, grafting density) on LCST; (4) uncovers modern characterization tools for precisely determining thermoresponsive properties (*e.g.*, LCST) and phase transition; and finally (5) touches on the state-of-the-art biomedical applications of thermoresponsive polymers with LCST transition.

## 2. Thermoresponsive polymers and their syntheses

### 2.1. Common types of thermoresponsive polymers

**2.1.1. Poly(*N*-substituted acrylamide)s.** Poly(*N*-substituted acrylamide)s and their copolymers have received significant attention due to the sharp phase transition and tunability of this value through the modification of pendant and end groups, incorporation of comonomers, or adjustment of the concentration. The most explored and researched member of this family is PNIPAM because of its LCST being quite close to body temperature making it suitable for biomedical applications. PNIPAM exhibits LCST around 32 °C, which is readily between room and body temperatures. The cloud point of PNIPAM decreases with increasing polymer concentration in water. However, it possesses some inherent issues, such as questionable biocompatibility<sup>81</sup> and phase transition hysteresis upon cooling (Fig. 2A).<sup>82</sup> During the transition regime, PNIPAM undergoes conformational changes involving intrachain coil-to-globule transitions and interchain self-association resulting in alteration in solubility and wettability. In this reversible phase transition process, at the temperature above LCST, PNIPAM exists in globular form. Most of the amide groups are covered, resulting in dehydration, and consequently, the polymer becomes more hydrophobic. Below the LCST, the extension of PNIPAM chains to a coil form is driven mainly by re-establishing the strong hydrogen bond interaction with the surrounding water molecules, rehydrating, and regaining hydrophilicity.<sup>83,84</sup>

Numerous reports described the synthesis and use of (co) polymers of PNIPAM with other functional comonomers such as other acrylamides,<sup>86</sup> (meth)acrylates,<sup>87,88</sup> ethylene glycols,<sup>57</sup> and pyrrolidines.<sup>89</sup> In addition, PNIPAM-based crosslinked hydrogel systems<sup>51,80</sup> and brushes<sup>72,90</sup> were explored. Because of its tunable LCST, PNIPAM or its copolymers have broad application prospects such as medical diagnostics, drug deliv-





**Fig. 2** Plots of transmittance as a function of temperature measured for aqueous solutions of (A) a PNIPAM homopolymer ( $DP_n$  ca. 100;  $M_w/M_n = 1.12$ ) (red) and (B) a copolymer P(MEO<sub>2</sub>MA-co-OEGMA) containing 5 mol% OEGMA per chain ( $DP_n$  ca. 100;  $M_w/M_n = 1.34$ ) (blue). Transmittance drops to 0% when the size of polymer aggregates becomes larger than the visible light and the solution turns completely opaque. Adapted with permission from ref. 85. Copyright 2006, American Chemical Society.

ery, biomedical devices, tissue engineering, and separations.<sup>91</sup> Thermosensitivity of poly(*N*-substituted acrylamide) derivatives with the substituents on the nitrogen atom on the side chain has also been studied.<sup>34</sup> Poly(*N*-alkylacrylamide)s (PAMs) such as poly(*N*-ethylacrylamide) (PNEAM), poly(*N*-cyclopropylacrylamide) (PNcPAM),<sup>92</sup> and poly(*N*-*n*-propylacrylamide) (PN<sub>*n*</sub>PAM),<sup>93</sup> and poly(*N,N*-dialkylacrylamide)s (PDAs) such as poly(*N,N*-ethylmethylacrylamide) (PEMAM),<sup>94</sup> poly(*N,N*-diethylacrylamide) (PDEAM),<sup>95</sup> poly(*N*-acryloylpyrrolidine) (PAPy),<sup>96</sup> and poly(*N*-acryloylpiperidine) (PAPi) undergo thermal phase transition in water. It was reported that the thermoresponsive properties depend on the degree of hydrophobicity, bulkiness, and flexibility of the substituents on the amide groups.<sup>26,34,97–99</sup> Fig. 3 shows the chemical structures and reported LCST or  $T_{cp}$  values of PNIPAM copolymers and poly(*N*-substituted acrylamide) derivatives.

**2.1.2. Ethylene glycol-based polymers.** The literature contains a wide range of poly(ethylene glycol)-based monomers (*i.e.*, monofunctional (meth)acrylic monomers with 5 or higher ethylene glycol units on the side chain) that are polymerizable, although LCST of ethylene glycol-based polymers are typically around 80–100 °C making it unsuitable for bio-related applications.<sup>100</sup> Yet, they have generated tremendous research attention, given their high biocompatibility and low toxicity. Methoxy-terminated (or methyl ether) oligo(ethylene glycol) (OEG) units are preferable due to displaying small or no hysteresis upon cooling (Fig. 2B) whereas hydroxy-terminated OEG units are preferable as they have an OH group at the chain end which can be modified to tune LCST.<sup>101,102</sup> Lutz *et al.* studied the LCST behavior of poly(2-(2-methoxyethoxy)ethyl methacrylate-co-oligo(ethylene glycol)methacrylate) (P(MEO<sub>2</sub>MA-co-OEGMA<sub>475</sub>)) copolymers, exhibiting a similar or superior thermoresponsive transition as compared to PNIPAM.<sup>85</sup> These P(MEO<sub>2</sub>MA-co-OEGMA<sub>475</sub>) copolymers showed a uniform and

sharp thermal profile with heating/cooling cycles. However, PNIPAM demonstrated a sharp transition upon heating and a broad hysteresis in the cooling process (Fig. 2A). This hysteresis is potentially from intra- and intermolecular hydrogen bonding within the dehydrated PNIPAM globules. On the other hand, OEGMA-based copolymers do not possess intermolecular hydrogen bonding and hence show minimal hysteresis. Additionally, the LCST of P(MEO<sub>2</sub>MA-co-OEGMA<sub>475</sub>) copolymers is nearly unaffected by the change in salt concentration, degree of polymerization, and polymer concentration (Fig. 4).<sup>85</sup> A variety of thermoresponsive OEGMA-based (co) polymers for use in practical biological applications were also highlighted by Lutz.<sup>103</sup>

Polymers containing carbon-carbon backbones (*e.g.*, acrylic, methacrylic, styrenic) with short ethylene glycol side chains (*e.g.*, mono-, di-, and tri-ethylene glycol) generally demonstrate lower LCSTs in aqueous solution than polymers with long ethylene glycol side chains (*i.e.*, OEG).<sup>104,105</sup> The hydrophobicity of the polymer increases as the length of the ethylene glycol units decreases due to the increase in the overall percentage of the hydrocarbon backbone. For instance, PMEO<sub>2</sub>MA with two EG units and PMEO<sub>3</sub>MA with three EG units exhibit LCST around 26 and 52 °C, respectively. On the other hand, POEGMAs with 4–10 EG units have transition temperatures in the range of 60–90 °C. To tune the LCST, short and long ethylene glycol (EG) (meth)acrylates can be copolymerized at different ratios of each monomer.<sup>106–109</sup> Fig. 5 shows representative interactions between P(MEO<sub>2</sub>MA-co-OEGMA<sub>475</sub>) copolymer and water molecules (top) and optical transparency of the aqueous solutions at 25 °C and 45 °C (bottom). Above LCST, P(MEO<sub>2</sub>MA-co-OEGMA<sub>475</sub>) copolymer becomes completely opaque due to the aggregation of large particles. Polymers can be decorated with ethylene glycol units on the side chain with various main chains composed of polymethacrylate (POEGMA),<sup>104,110</sup> polyacrylate (POEGA),<sup>45</sup> polystyrene (POEGSt),<sup>111</sup> poly(vinyl ether) (POEGVE),<sup>112</sup> polynorbornene (POEGNB),<sup>113</sup> polyether (POEGE),<sup>114,115</sup> polylactide (POEGLA),<sup>116,117</sup> polymethylene (POEGM),<sup>118</sup> polyphosphazene (PBEEP),<sup>119,120</sup> and poly(amino acid)<sup>121,122</sup> (Fig. 3). These thermoresponsive polymers can be tailored as linear or branched as well as three-dimensional structures.<sup>34,123</sup> In addition, poly(ethylene oxide) (PEO) and poly(propylene oxide) (PPO) and their copolymers with LCSTs varying from 20 °C to 85 °C contain EG units in their main chains and are commercially available under the names of Pluronics, Poloxamers, and Tetronics.<sup>124–126</sup> Amphiphilic balance in OEG structure is the main reason for the thermoresponsive property of these types of polymers.<sup>127,128</sup>

The previous reports on thermoresponsive polymers are dominated by PNIPAM and POEGMA derivatives. However, a wide variety of other polymers demonstrated promising thermoresponsive behavior in aqueous solution.<sup>129–135</sup> For example, poly(*N*-vinylcaprolactam) (PNVCL)<sup>136–138</sup> and poly(oxazoline)s<sup>139–143</sup> have been recognized as synthetic polymers exhibiting LCST behavior.<sup>26</sup> Similar to PNIPAM, PNVCL is hydrophilic and soluble in water at room temperature, gradu-





Fig. 3 Chemical structures of common thermo-responsive homo- and co-polymers and their reported LCST or cloud point values.

ally becoming more hydrophobic and eventually insoluble in water when the temperature is raised from 25 °C to 35 °C.<sup>124</sup> Moreover, there are several examples of thermo-responsive

polymer-biopolymer conjugates to incorporate responsive behavior to the biopolymers such as cyclodextrin,<sup>144</sup> enzymes,<sup>145</sup> proteins,<sup>146</sup> or oligonucleotides<sup>124</sup> for target applications.







**Fig. 4** Molecular structures of ethylene glycol-based copolymer and PNIPAM (top). Plots of measured cloud points as a function of (A) NaCl concentration, (B) degree of polymerization (DP<sub>n</sub>), and (C) polymer concentration (bottom). In all figures, cloud points of P(MEO<sub>2</sub>MA-co-OEGMA<sub>475</sub>) and PNIPAM are represented by blue dots and red squares, respectively. Data in figures (A) and (C) were measured with a copolymer P(MEO<sub>2</sub>MA-co-OEGMA<sub>475</sub>) containing 5 mol% OEGMA<sub>475</sub> per chain (DP<sub>n</sub> ca. 100;  $M_w/M_n = 1.34$ ) and a homopolymer of NIPAM (DP<sub>n</sub> ca. 100;  $M_w/M_n = 1.12$ ). Adapted with permission from ref. 85. Copyright 2006, American Chemical Society.

## 2.2. Polymerization techniques and property control

**2.2.1. Solution polymerization.** Thermoresponsive polymers can be synthesized through several polymerization methods such as atom transfer radical polymerization (ATRP),<sup>34</sup> reversible addition-fragmentation chain transfer (RAFT) polymerization,<sup>147</sup> nitroxide-mediated polymerization (NMP),<sup>148</sup> ring-opening metathesis polymerization (ROMP),<sup>113</sup> group transfer polymerization (GTP),<sup>149,150</sup> ring-opening polymerization,<sup>151</sup> and anionic polymerization.<sup>104</sup> CRP techniques (*e.g.*, ATRP and RAFT polymerization) have been explored to a great extent due to the availability of the monomers and relatively simple reaction setup (Scheme 1). Additionally, these techniques enable the synthesis of polymers with controlled molecular mass, narrow molecular mass distribution or dispersity ( $D$  below 1.2–1.3), high end-group

fidelity (allowing block copolymer synthesis), and different architectures (*e.g.*, multi-block, star, comb).<sup>110,152</sup> In this section, only ATRP<sup>153–155</sup> and RAFT polymerization<sup>156–158</sup> to yield thermoresponsive polymers will be covered to give the readers a brief overview of these techniques and how to control structural features.

Acrylamides and (meth)acrylates can be successfully polymerized through ATRP and RAFT polymerization. Conventional ATRP can be used to polymerize most of the (meth)acrylates. However, the ATRP technique needs to be modified to be able to polymerize (meth)acrylamide-based monomers with high yield and narrow dispersity. As a typical methacrylate example, OEGMA was copolymerized with more hydrophobic MEO<sub>2</sub>MA or poly(propylene glycol methacrylate) (PPGMA) through conventional ATRP to decrease the LCST to below 37 °C.<sup>85,159</sup> Conventional ATRP requires a metal catalyst (*e.g.*, CuBr or CuCl), a ligand (*e.g.*, linear amines or bipyridines), and an initiator (*e.g.*,  $\alpha$ -haloester).<sup>153</sup> Several (meth)acrylamides (*N,N*-dimethylacrylamide, *N-tert*-butylacrylamide, and *N*-(2-hydroxypropyl)methacrylamide) were attempted to polymerize through conventional ATRP. When linear amines and bipyridines were employed as ligands in bulk or solution, very low monomer conversions were obtained. The low conversion can be attributed to the copper catalyst competitively complexing with poly(meth)acrylamides. The use of 1,4,8,11-tetramethyl-1,4,8,11-tetraazacyclotetradecane (Me<sub>4</sub>Cyclam) as a ligand resulted in high yield in a short period of time, but the polymerization was not controlled potentially due to the slow deactivation and the loss of bromine end groups due to side reactions, yielding high dispersity.<sup>152</sup> Masci *et al.* reported a successful ATRP of NIPAM using tris[2-(dimethylamino)ethyl] amine (Me<sub>6</sub>TREN) as a ligand, ethyl 2-chloropropionate as an initiator, CuCl as a catalyst in dimethylformamide (DMF)/water (1 : 1, v/v) at room temperature (Scheme 1A). The reaction yielded a first-order kinetic plot with 92% conversion and dispersity of 1.19.<sup>160</sup> Supplemental activator and reducing agent (SARA) ATRP in the presence of Cu<sup>0</sup> and electrochemically mediated ATRP (*e*ATRP) of NIPAM were also previously investi-

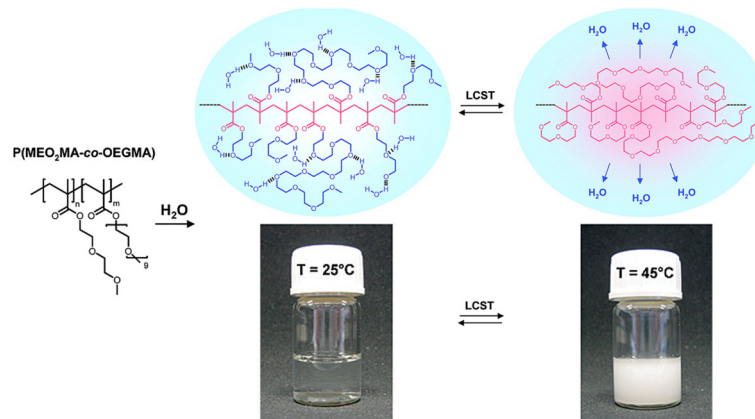


**Fig. 5** Proposed mechanism for the temperature-induced phase transition of poly(MEO<sub>2</sub>MA-co-OEGMA) copolymers in aqueous solution. Adapted with permission from ref. 106. Copyright 2007, American Chemical Society.





**Scheme 1** Synthetic schemes for ATRP and RAFT polymerization of acrylamide monomers.

gated. PEO-*b*-PNIPAM copolymers were successfully synthesized with narrow dispersity and the % conversion between 43–95% by SARA ATRP and *e*ATRP.<sup>161</sup> Moreover, activators regenerated by electron transfer (ARGET) ATRP<sup>162</sup> can be utilized to synthesize thermoresponsive polymers from (meth) acrylic and (meth)acrylamide monomers (Scheme 1A). ARGET ATRP is a robust technique that is less sensitive to oxygen presence and requires Cu<sup>II</sup> catalyst and a reducing agent such as tin(II) 2-ethylhexanoate (Sn(EH)<sub>2</sub>) or ascorbic acid. For the synthesis of PNIPAM, more active catalyst systems with a tetradentate ligand such as Me<sub>6</sub>TREN or tris(2-pyridylmethyl)amine (TPMA) which is 10<sup>3</sup>–10<sup>5</sup> times more active than CuBr/bipyridine complexes are necessary.<sup>162</sup> It should be noted that the potential toxicity of residual transition metal catalyst contamination is the key limiting factor for applications of thermoresponsive polymers synthesized *via* ATRP. The use of more active catalysts to lower the catalyst loading and more rigorous purification for the removal of metals after polymerization is critical for biomedical applications.<sup>163–165</sup> Precisely controlled molecular architecture (topology, composition, functionality) of polymers, hybrid materials, and bioconjugates can also be achieved through ATRP.<sup>166–170</sup>

RAFT polymerization has been widely used to synthesize thermoresponsive polymers from various types of monomers. RAFT polymerization can allow metal-free synthesis of these responsive polymers; however, cytotoxicity of the chain transfer agent (CTA) remaining at the end of the polymer chains was reported.<sup>171–173</sup> The end group CTAs also need to be completely removed to prevent any complications.<sup>174,175</sup> In early 2000, a series of PNIPAM homopolymers were synthesized by using benzyl and cumyl dithiobenzoate (Scheme 1B) in different organic solvents (benzene and 1,4-dioxane) at 60 °C.<sup>176,177</sup>

Convertine, McCormick, and co-workers successfully polymerized NIPAM through the RAFT process at room temperature. A commercial trithiocarbonate RAFT CTA, 2-(dodecylsulfanylthiocarbonylsulfanyl)-2-methylpropionic acid, along with an azo initiator, 2,2'-azobis(4-methoxy-2,4-dimethylvaleronitrile) (V-70) was used to homopolymerize NIPAM in DMF at 25 °C. PNIPAM homopolymers with *M<sub>n</sub>* of *ca.* 50 000 g mol<sup>−1</sup> and dispersity of *ca.* 1.10 were obtained. These homopolymers were then used as a macroCTA to yield block copolymers. Near-quantitative block copolymer formation with narrow dispersity was confirmed by size-exclusion chromatography (SEC).<sup>178</sup> The same research group synthesized thermoresponsive *N,N*-dimethylacrylamide (DMA)/NIPAM di- and tri-block copolymers *via* aqueous RAFT polymerization at room temperature.<sup>179</sup> Overall, trithiocarbonate RAFT agents (Scheme 1B) were reported as a more versatile CTA for more activated monomers such as acrylamides.<sup>180</sup> RAFT polymerization of various *N*-alkylacrylamide and *N,N*-dialkylacrylamide derivatives was reviewed by Kakuchi *et al.* in 2022. Kanaoka and co-workers synthesized PNIPAM hydrogels *via* a polymerization-induced self-assembly process in which they employed PDMA as macroCTA and a divinyl cross-linker. Their research group also reported PNIPAM-based crosslinked hydrogel being formed in a star shape and observed greater dispersibility and uniform distribution of the star PNIPAM polymers at the crosslinking point.<sup>181</sup> Other thermoresponsive star architectures synthesized through RAFT process have also been reported.<sup>182–185</sup>

Thermoresponsive polymers can also be made through photo-polymerization methods. Photo-induced electron/energy transfer (PET)-RAFT polymerization in the presence of a photo-redox catalyst which transmits the captured light energy to the



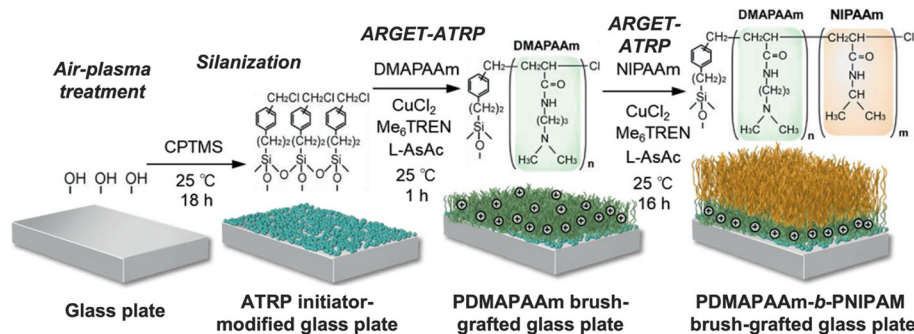


**Fig. 6** Preparation of a thermoresponsive block copolymer brush-modified glass plate through ARGET ATRP. Adapted with permission from ref. 90. Copyright 2020, John Wiley and Sons.

CTA has been widely used.<sup>186</sup> Photoiniferter (PI)-RAFT polymerization, on the other hand, involves direct photolytic cleavage of a CTA by the light, after which the procedure is changed to available RAFT mode. Corrigan, Boyer, and co-workers prepared PNIPAM homopolymers *via* PET-RAFT polymerization. 2-(*n*-Butyltrithiocarbonate) propionic acid as a CTA and 5,10,15,20-tetraphenyl-21*H*,23*H*-porphyrin zinc(II) (ZnTPP) as a photo-redox catalyst were used to polymerize NIPAM in methanol under green LED light ( $\lambda_{\text{max}} = 520$  nm) and inert atmosphere. Polymers with narrow dispersity ( $D < 1.18$ ) and  $M_n$  ranging from 6.3–66.2 kg mol<sup>−1</sup> were synthesized for cloud point comparison.<sup>187</sup> Karpov and co-workers reported dimethyl sulfoxide (DMSO) as the best solvent for homopolymerization among other solvents (DMSO > tetrahydrofuran, THF > toluene) for photo-RAFT polymerization. Amphiphilic random and diblock alkoxy (C<sub>12</sub>–C<sub>14</sub>) OEGMA (with *ca.* EG units) and methoxy-OEGMA<sub>500</sub> (1 : 1) bottlebrush copolymers have been synthesized by means of PI-RAFT polymerization in different solvents. Moreover, the authors performed an “on–off” experiment to confirm the easy switchability of the process and pseudo-living mechanism of polymerization.<sup>188</sup>

**2.2.2. Surface-initiated polymerization.** Grafting polymers is beneficial to tune surface properties such as wettability, corrosion resistance, and friction.<sup>189–191</sup> Polymer coatings on a substrate can be generated by chemical bonding or physical adsorption.<sup>192</sup> Chemisorption is a favorable strategy over physisorption for biomedical application as it does not result in desorption into a physiological environment and offer superior chemical modification control.<sup>193</sup> “Grafting-to” approach can be utilized for chemical coupling between reactive end groups of polymer and reactive groups on the surface.<sup>194,195</sup> Polymers can be anchored to the surface this way by a chemical reaction between the end groups on the polymers and functional groups on the surface. The “grafting-to” entails synthesizing polymer chains separately before attaching them to the surface. The polymer chains or brushes can be grown *in situ* from initiators that have been fixed to the surface in the “grafting-from” method (as employed in Fig. 6). Among these synthetic pathways, the “grafting-from” approach is considered an efficient technique to precisely control the functionality,

polymer grafting density, dispersity, and thickness of polymer brushes (*i.e.*, grafting length).<sup>196–199</sup> Moreover, controlled surface-initiated (SI)-polymerization can be employed from different surface materials, such as silicon, glass, gold, alloys or metal-oxides, mica, graphene, cellulose, and nanoparticles.<sup>200</sup> A controlled polymerization is highly preferred in order to provide closer control of the architectural features of the resulting brush. Based on radical chemistry, there are many SI-controlled radical polymerization techniques: SI-ATRP,<sup>201–203</sup> SI-RAFT polymerization,<sup>204,205</sup> SI-NMP,<sup>206</sup> SI-PET-RAFT polymerization,<sup>207–209</sup> and SI-PI-mediated polymerization.<sup>210</sup> Nagase *et al.* demonstrated the synthesis of a thermoresponsive cationic block co-polymer, *N,N*-dimethylaminopropylacrylamide (PDMAAm)-*b*-PNIPAM by SI-A(R)GET ATRP from a glass plate as a useful cell separation tool (Fig. 6).<sup>90</sup> In addition, poly(*N*-(2-methacryloyloxyethyl)pyrrolidone) (PNMEP) surface-adhered brushes were reported by Teunissen *et al.* through SI-ATRP from silicon oxide-coated silicon surfaces.<sup>201</sup> Notably, SI-ATRP has evolved to be a dominant synthetic technique to prepare surface-initiated polymer brushes because of simple experimental requirements, its versatility, more uniform grafting length, and tolerance toward a wide spectrum of functional monomers.

### 3. Effects of structural heterogeneity on LCST

A hydrophilic–hydrophobic balance in the thermoresponsive polymer chains gives rise to changing their shape (*i.e.*, random coil to globule) in response to temperature change. To finely tune the LCST of thermoresponsive polymers, several structural factors have been investigated including architectures, compositions, molecular mass, dispersity, and grafting length/density.

#### 3.1. Architectures

The responsive properties can be manipulated by changing the macromolecular architectures. Thermoresponsive polymers with different macromolecular architectures, such as block, cyclic, comb, bottlebrush, and star, have been synthesized



using controlled/living polymerization techniques and the structural effects on thermal phase transition have been studied. Different polymer architectures used for thermo-responsive polymer design (A–E) and multi-arm star and hyperbranched copolymers with PEG side chains (F and G) are shown in Fig. 7.<sup>3,211</sup> For PEG-based polymers, the differences in thermal behavior between block and gradient copolymers of 2-hydroxyethyl acrylate (HEA) and ethylene glycol methyl ether acrylate (mEGA) were reported by Steinhauer *et al.*<sup>212</sup> The  $T_{cp}$  was shown to be tuned between 0 °C and 80 °C for the block copolymers and between 0 °C and 60 °C for the gradient copolymers. Sun *et al.* studied a reversible polymer architecture switching process between linear polymers and cross-linked nanogels. By investigating multifunctional block copolymers of acrylamide and ethylene glycol acrylate derivatives, they found that linear structures showed sharp thermal transitions while the crosslinked nanogels showed linear thermal transitions over a broad temperature range.<sup>213</sup> For other polymer systems, the relationship between thermoresponsive behaviors and architectures is also demonstrated. Cheng *et al.* prepared a series of poly(3-ethyl-3-(hydroxymethyl)-oxetane) (PEHO)-*star*-PEO and PEHO-*star*-poly(2-(dimethylamino)ethyl methacrylate) (PDMAEMA) copolymers.<sup>211</sup> The LCST transition of the first system is based on hydrophilic–hydrophobic balance and is highly dependent on the degree of branching of the PEHO core. EG-based polymers were synthesized in star–block architectures to produce thermoreversible hydrogels (thermogels or hydrogelators). MEO<sub>2</sub>MA and OEGMA<sub>475</sub> were copolymerized using a 4-arm star PEG ATRP macroinitiator. These star–block

copolymers with an inner PEG core and outer block thermo-responsive arms exhibited drastic changes in viscosity above LCST. The star copolymers showed a reversible thermogelation within the range of 35–42 °C over repeated heating/cooling cycles as opposed to the linear block copolymer solutions which only displayed a higher viscosity upon heating.<sup>214,215</sup> Li *et al.* synthesized dendrimers containing PEG in the main chain, and OEG as a side chain.<sup>216</sup> With an aim to examine how the length of the OEG side chain affects the thermo-responsive behavior, the research group of Deng synthesized a series of degradable copolymers with varying EG units from 1 to 3.<sup>217</sup> Moreover, EG-based polymers exhibit a broad thermo-responsive behavior in dendronized form. For instance, OEG-based dendrons display hitherto unseen abrupt and rapid transitions in aqueous solution with LCSTs varying from 27 to 65 °C.<sup>216</sup>

PNIPAM-based block copolymers and star polymers containing hydrophilic or hydrophobic segments exhibit various LCSTs (Fig. 3).<sup>218–222</sup> A series of PNIPAM- and PDMA-based double hydrophilic multiblock copolymer architectures with hydrophobic dodecyl hydrocarbon end-groups were synthesized through RAFT polymerization. It was shown that incorporations of hydrophilic comonomer can increase the  $T_{cp}$  of the block copolymer systems.<sup>223</sup> Lang *et al.* prepared ethyl- and dodecyl-terminated PNIPAM, PN<sub>n</sub>PAM, and PNC<sub>n</sub>PAM to unveil the relationship between chain terminal groups and thermoresponsive behaviors.<sup>224</sup> When below the critical temperature, polymers terminated with short hydrophobic groups would have large-scale, fractal assemblies while polymers with long hydrophobic terminal groups formed small micelles. As expected,  $T_{cp}$  of PNIPAM decreases when the polymer is decorated with hydrophobic end groups and the opposite effect can be observed when the end groups are hydrophilic.<sup>225</sup> The star and cyclic architectures have been shown to affect thermo-responsive behavior, especially polymers with low molecular masses. Polarity of the core and end-groups and the number and length of the arms directly affect the thermoresponsive properties in the star architecture.<sup>226,227</sup> PNIPAM-based star polymers showed lower  $T_{cp}$  (Fig. 8), and cyclic polymers showed higher  $T_{cp}$  compared with linear structures.<sup>34</sup> The  $T_{cp}$  values of four-arm star PNIPAM were reported lower than those of linear counterparts.<sup>228</sup> When working as a thermo-responsive shell of core–shell copolymers using tris(2-aminoethyl)amine (TREN) and a polyamido-amine hyperbranched polymer as the core,  $T_{cp}$  increased as the degree of branching increased.<sup>229</sup> Winnik *et al.* reported the effects of cyclic architecture on the phase transitions of PNIPAM systems in aqueous solutions. Linear PNIPAMs with  $\alpha$ -azido and  $\omega$ -propargyl end-groups were synthesized through RAFT polymerization and subsequently, these end groups were clicked *via* aminolysis/Michael addition reactions to yield cyclic PNIPAM polymers.<sup>230</sup> It was reported that polymer concentration and structural factors such as the absence of end groups and steric hindrance, affect the phase transition for cyclic PNIPAM systems.<sup>231</sup> PNIPAM copolymers with different compositions and architectures (*e.g.*, random, block, graft, or

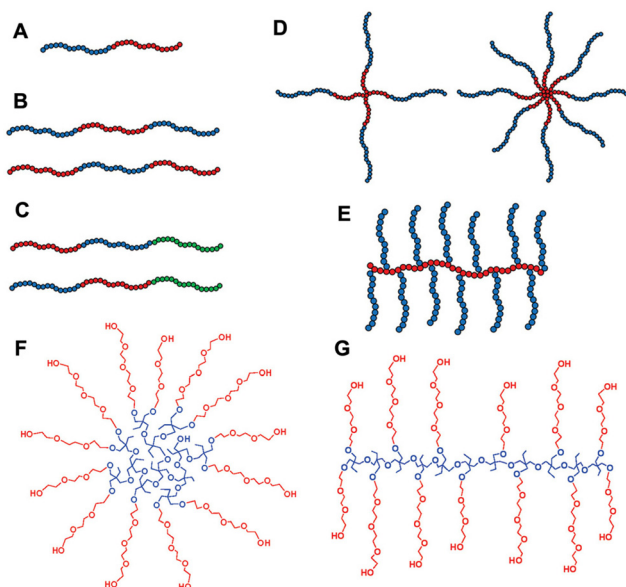


**Fig. 7** Polymer architectures used in the construction of thermoreversible polymers: (A) Di-block, (B) ABA tri-block, (C) ABC tri-block, (D) 4 and 8-arm star-shaped, (E) graft copolymers. (F and G) Multi-arm star and hyperbranched copolymers with poly(ethylene oxide) side chains. Adapted with permission from ref. 3 and 211. Copyright 2020, John Wiley and Sons and 2010, American Chemical Society.







**Fig. 8** Structures and thermo-responsive properties of linear and four-arm star-shaped PNIPAM at different molecular weights. Reproduced with permission from ref. 34. Copyright 2022, RSC.

star) have been also shown to exhibit a sol-gel transition upon heating.<sup>232–236</sup>

### 3.2. Molecular mass and dispersity

Phase transition of thermo-responsive polymers from coil to globule in aqueous solutions is considered a function of molecular mass and  $\bar{D}$ . This is especially relevant regarding synthetic polymers, whose molecular mass and  $\bar{D}$  can be altered and controlled to manipulate the corresponding thermo-responsive behavior. The molecular mass dependency of the  $T_{cp}$  of PNIPAM was reported by Stöver *et al.* Polymers with  $M_w$  ranging from 2800 to 26 500 g mol<sup>-1</sup> with narrow dispersity ( $\bar{D} = 1.1$ – $1.2$ ) were prepared by the ATRP technique. Turbidimetry and differential scanning calorimetry studies showed that the  $T_{cp}$  of the PNIPAM aqueous solutions decreased as the molecular mass increased. This inverse relationship between the  $T_{cp}$  and molecular mass has also been reported for other poly(*N,N*-dialkyl acrylamide)s (Fig. 9).<sup>94,237–239</sup> Liu *et al.* synthesized a semirigid water-soluble thermo-responsive polymer and found that both the monomer bis(*N*-hydroxyisopropyl pyrrolidone) 2-vinylterephthalate (HIPPVTA) and PHIPPVTA exhibited thermo-responsive phase transition behaviors in aqueous solutions and that PHIPPVTA exhibited an increased  $T_{cp}$  with increasing molecular mass.<sup>240</sup> PHIPPVTA cloud point is extremely dependent on  $M_w$  and  $\bar{D}$ , while it also demonstrates a great solvent isotopic effect. The effect of molecular mass and  $\bar{D}$  on thermal behaviors can also be seen in synthetic polymer mixtures. Corrigan, Boyer, and co-workers prepared a series of PNIPAM homopolymers with narrow dispersity *via* PET-RAFT

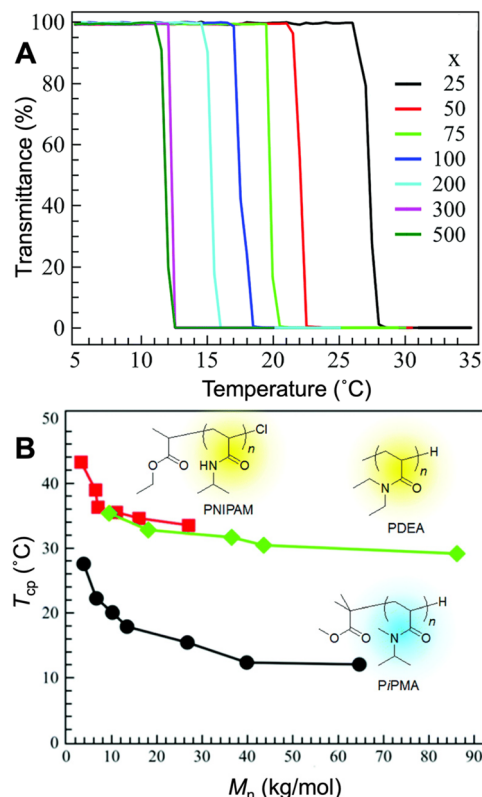


**Fig. 9** (A) The cloud point curves (transmittance vs. temperature) of poly(*N,N*-isopropylmethylacrylamide) (PiPMA) with different degrees of polymerization ( $x$ ) in aqueous solution. (B) The molecular mass dependence of cloud point temperature of PNIPAM (■), poly(*N,N*-diethylacrylamide) (PDEA) (◆), and PiPMA (●). Adapted with permission from ref. 34, 225, 237 and 242. Copyright 2020 and 2022, RSC and 2019 and 2005, American Chemical Society.

polymerization. Their study showed that the cloud points are inversely proportional to the  $M_w$ . For binary blends of PNIPAM homopolymers with more highly skewed dispersity and large tailing, they determined that the thermo-responsive behavior changed from a single, sharp transition to a broad transition, and eventually to two distinct transitions.<sup>187</sup> While this study is limited to PNIPAM samples, it illustrates the effect of the shape of dispersity on the thermal responsive behavior of polymer mixtures. PEGMA copolymer mixtures also demonstrated the effect of  $M_w$  and  $\bar{D}$  on the thermo-responsive behaviors, supporting this idea that the thermo-responsiveness of polymer mixtures is dependent on  $M_w$  and  $\bar{D}$ . Through synthesizing triblock copolymers with a PEGMA, *n*-butyl methacrylate (*n*BuMA), and DMAEMA block and with varying molecular mass and composition, Ward *et al.* demonstrated that composition influenced the  $pK_a$  and that both molecular mass and composition influenced the cloud point, hydrodynamic diameter, and gelation of the polymers.<sup>241</sup> These results suggest that the composition and molecular mass of triblock polymers can be manipulated with the promise of gel-formation abilities due to their thermo-responsive behavior. Overall, understanding the effect of molecular mass and  $\bar{D}$  on polymers is crucial



in developing polymeric thermoresponsive materials for drug delivery and tissue engineering.

### 3.3. Grafting length/density

Grafting density has also proved to influence the thermoresponsive behaviors of polymers. PNIPAM is the most studied regarding grafting effects as it experiences a conformational change above its LCST and the physical properties of PNIPAM are readily altered by changing the temperatures even when grafted to surfaces. Both graft length and density were discovered to impact thermoresponsive behavior and self-assembly morphology. Jiang *et al.* determined that both graft length and density experienced a positive correlation with LCST, mean diameter, and size distribution, with graft length having a more significant effect than density, and that graft length and density had a more significant effect on diameter than self-assemble morphology.<sup>243</sup> The grafted polymers with dense side chains and higher molecular masses had higher LCSTs with the aggregates having bigger diameters and stronger steric repulsive interactions. Thus, the desired thermoresponsive behavior and self-assembly morphology can be achieved by altering the grafting length and grafting density to the proper length. When looking at the effect of grafting on thermoresponsive polymers, the effect of molecular mass should also be considered because the magnitude of the conformational changes is usually dependent on size. Yim *et al.* studied the temperature-dependent conformational changes of PNIPAM chains grafted over a range of grafting lengths and densities. They found that the conformational change of the grafted PNIPAM brushes varied greatly with molecular mass and grafting density, with the maximum conformational change observed for the brushes with high molecular mass and intermediate grafting density.<sup>244</sup> This is due to the competition between the stretching effect of laterally interacting tethered chains. Moreover, molecular mass and grafting density were also found to affect the collapse of these end-grafted PNIPAM polymers above the LCST. Plunkett *et al.* observed thermally induced chain collapse at a high molecular mass and high grafting density.<sup>245</sup> It was concluded that PNIPAM behaves as an ideal polymer (*i.e.*, the same distribution was observed with a different effective bond length) at and above the LCST but not below the LCST. Overall, the ability to tune the thermal properties of PNIPAM films depends strongly on the grafting parameters.

Other external components along with temperature influence the thermoresponsive behavior of polymers, the main being pressure, salts, and buffers since hydrogen bonding ability or other electrostatic interactions in solution can be affected. The pressure was found to induce structural changes, transitioning from coil to globule.<sup>246</sup> The effect of salt types and concentrations on the thermal transitions of non-ionic POEGMA-based copolymers synthesized *via* ATRP was investigated. The LCST of the copolymer increased or decreased depending on the salt type.<sup>247</sup> Dendritic polymers were found to be more sensitive to the addition of salt, experiencing a nonlinear decrease in LCSTs with rising salt concentrations.<sup>248</sup>

The specific type of ion affects the LCST as thermoresponsive polymers experience decreasing LCST with increasing kosmotropic (water “structure maker”) anion concentration and abnormal salting out properties at low chaotropic (water “structure breaker”) concentrations.<sup>249</sup> The type of ion has also been found to affect the structure of polymer brushes, with kosmotropes resulting in relatively collapsed structures whereas chaotropes resulting in relatively swollen structures.<sup>250</sup> The presence of salt in buffer solutions was determined to be non-additive, and the influence of salt on polymer aggregation was dependent on salt ion type, concentration, and polymer main chain structure.<sup>251</sup>

## 4. Characterization of thermoresponsive behavior

General characterization techniques to confirm successful syntheses of thermoresponsive polymers usually include Nuclear Magnetic Resonance (NMR) spectroscopy, Size-Exclusion Chromatography (SEC), and UV-Vis and Fourier transform infrared (FTIR) spectroscopy techniques. To better understand the LCST behavior, other advanced characterization techniques will be introduced in this section. We categorized these techniques into two parts: solution characterization and bulk characterization. An overall summary of these characterization techniques is given in Table 1.

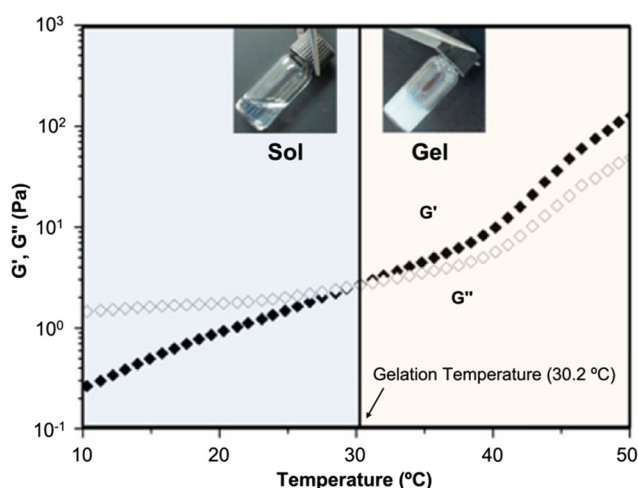
### 4.1. Solution characterization

**4.1.1. Rheological studies.** Rheology is an important technique to study of thermoresponsive behavior of polymers because the flow (*i.e.*, complex viscosity) and mechanical properties of these materials can change significantly with temperature. This technique can also be performed in bulk depending on the glass transition temperature and physical state of the polymer at room temperature. Polymer solutions and polymer melts are expected to show lower viscosity at a higher temperature. However, polymer solutions with LCST behavior show higher viscosity with increasing temperature.<sup>288</sup> The rheological properties of thermoresponsive polymers under applied shear at different temperatures are very critical since it provides a quantitative method to show the relationship between mechanical properties and internal structures and helps in the understanding of phase transition behavior, viscoelasticity, and time-temperature superposition. The shear storage modulus/elastic modulus ( $G'$ ) and shear loss modulus/viscous modulus ( $G''$ ) can be measured by using a rheometer and sol-gel transition (a gel point) is observed when  $G'$  becomes larger than  $G''$  (Fig. 10).<sup>289</sup> Cook and co-workers investigated the temperature-dependent rheology of thermoresponsive EG-based graft copolymers. Rheology was performed with poly(DEGMA-*co*-OEGMA), poly(NIPAM-*co*-OEGMA), and poly(DEA-*co*-OEGMA) (OEGMA,  $M_n = 500$  or  $2000 \text{ g mol}^{-1}$  and methoxy or hydroxy terminus) at 25% (w/w) concentration. All three polymers exhibited an increase in viscosity (thermothickening) around their respective cloud



**Table 1** Solution and bulk characterization techniques for thermoresponsive polymers

Characterization technique	Results collected	Polymers tested	Ref.
<b>Solution characterization</b>			
Rheological studies	Phase transition behavior, viscoelasticity, and time-temperature superposition	PNVCL, PNIPAM, PDMAEMA, POEGMA	52, 229, 241 and 252
Optical studies	Cloud point measurement: temperature of phase inversions in polymer solutions	POEGMA, PNIPAM, EG-PLLA, EG-PDLA, P(OEGA)- <i>co</i> -(DEGA), PDMA- <i>b</i> -P(MEA- <i>co</i> -PEGA- <i>co</i> -PDSEA- <i>co</i> -Flu)	97, 213 and 253–256
Light scattering measurements	Size distribution profile of polymers in solution	P(NVCL/VP), poly(OEGMA- <i>co</i> -DEGMA), P(OEGMA- <i>co</i> -HMS <i>t</i> BA), P(DEGMA- <i>co</i> -HPMA- <i>co</i> -PEGMA), PDMA- <i>b</i> -P(NIPAM- <i>co</i> -ACPBA), P(DEGMA- <i>co</i> -HPMA), PNIPAM, P(DMA- <i>b</i> -(NIPAM- <i>co</i> -DMAEA- <i>co</i> -BA)), PDEA	182, 252 and 257–264
Small-angle scattering (SANS/SAXS)	Shape and organization of large molecules, conformational polydispersity	PNIPAM, P(DEGMA)	254 and 265–267
Diffusion coefficients measurements	Hydrodynamic radius, formation of aggregated species	Hyperbranched poly(ethylene imine), OEG	229, 268 and 269
<b>Bulk characterization</b>			
Contact angle measurements	The contact angle between polymer surfaces and a water droplet	PMEO <sub>2</sub> MA, P(MEO <sub>2</sub> MA- <i>co</i> -OEGMA), PNIPAM, PN <i>t</i> BAM, poly(NIPAM- <i>co</i> -N <i>t</i> BA)	270–272
Ellipsometry	The thickness of polymer films	PMEO <sub>2</sub> MA, P(MEO <sub>2</sub> MA- <i>co</i> -OEGMA), PNIPAM, P(MEO <sub>2</sub> MA- <i>stat</i> -OEGMA), PNIPAM- <i>g</i> -PEG	270, 271, 273 and 274
Thermal analysis (DSC, TGA)	Identification of physical properties and thermal transitions of polymers	P(NVCL/VP), PNIPAM-based polymers, pMPEGMA, pAOEGMA, PEGMA- <i>b</i> -PBuMA- <i>b</i> -PDMAEMA, poly(2-isopropyl-2-oxazoline)	229, 241, 252 and 275–283
Electron microscopy (SEM, TEM)	Particle counting, size determination, topography, and atomic composition	P(VP- <i>stat</i> -NVCL), PNIPAM, P2VP-PEO	229, 252 and 284
X-ray photoelectron spectroscopy (XPS)	Composition of surface material elements and their relative abundance, chemical state of the polyvalent ions	PNIPAM, OEGA-based polymers, poly(2-isopropyl-2-oxazoline)	201, 256, 285 and 286
Atomic force microscopy (AFM)	Adhesion strength, magnetic forces, mechanical properties, topography	Poly(NIPAM- <i>co</i> -acrylamidebenzophenone (AcBzPh)) poly(NIPAM- <i>co</i> -AcBzPh- <i>co</i> -N- <i>tert</i> -butylacrylamide), PNIPAM, poly(2-isopropyl-2-oxazoline)	76, 101, 281, 285 and 286
X-ray powder diffraction (XRD)	Degree of crystallinity and phase ratio	PNIPAM, $\beta$ -cyclodextrin thermoresponsive diblock copolymer	283 and 287

**Fig. 10** Thermogelling behavior at LCST. Dynamic rheological analysis of a thermoresponsive copolymer in aqueous solution as a function of temperature. Reprinted with permission from ref. 289. Copyright 2012, American Chemical Society.

points. It was reported that copolymer systems with methoxy-terminated OEGMA units formed stable colloidal structures above LCST, and poly(DEGMA-*co*-OEGMA) showed the thermal transition between room and body temperature, which is desired for biological applications.<sup>290</sup> Iohara *et al.* studied the

thermoresponsive reversible sol-gel transition of hydrophobically modified hydroxypropyl methylcellulose/cyclodextrin hydrogels.<sup>52</sup> Rheological measurements were used to show how temperature and the added amounts of cyclodextrin would affect the viscosity of the hydrogel. In another study, for PNVCL-based hydrogels,  $G'$  and  $G''$  change upon the temperature for the PNVCL homopolymer.<sup>252</sup> Their results showed a sol-gel transition at 36 °C. The  $G'$  and  $G''$  were also measured for PNVCL-*stat*-poly(vinylpyrrolidone) (PVP) copolymers with different compositions to rationalize the improved hydration phenomenon of this family of polymers. Rheological techniques were also used to quantify the mechanical changes during the sol-gel transition of TREN- and PNIPAM-based hydrogels.<sup>229</sup> These hydrogels were made from hyperbranched polymers with a thermoresponsive shell and they got stiffer with a slower sol-gel transition as the degree of branching increased. Ward *et al.* systematically studied how molecular mass and composition affect the gelation of thermoresponsive polymers by using temperature sweep rheology.<sup>241</sup> They prepared ABC triblock copolymers using non-ionic hydrophobic *n*BuMA, ionizable hydrophilic and thermoresponsive DMAEMA, and non-ionic hydrophilic methoxy PEGMA monomers. The gel points of polymer solutions in phosphate-buffered saline were tested. They concluded that the gel point decreases when the molecular mass and the hydrophobic content increase.



**4.1.2. Optical studies.** Turbidimetry is an efficient and arguably the most common way to study the phase transition of thermoresponsive polymers and is utilized to analyze the cloud points of the polymer solutions by using a UV-Vis spectrometer.  $T_{cp}$  is the temperature at which the polymer undergoes a coil-to-globule transition from a soluble state to an insoluble, aggregated state in a particular solvent at a specific concentration. The solution turns turbid when the size of the globules becomes larger, and the visible light will be scattered as it passes through the solution. Typically, the  $T_{cp}$  is reported as the temperature at which 50% transmittance is observed in a UV-Vis spectroscopy analysis (Fig. 11A).<sup>253</sup> As the concentration of the polymer in the solution increases, the  $T_{cp}$  typically decreases until reaching the minimum value in the temperature-concentration phase diagram, which is defined as LCST. The  $T_{cp}$  response depends on the properties of the polymer and the solution, as well as the rate of heating.<sup>291,292</sup> In general, the  $T_{cp}$  response is fast on the order of seconds to minutes. Results from this turbidity measurement play a critical role in understanding the performance and functionality of thermoresponsive polymers because the phase transition can get triggered by the changes in the physical properties of the polymer. In many applications, the  $T_{cp}$  is adjusted to match the temperature range for the desired design and optimization of thermoresponsive systems, allowing for precise control over the behavior of the polymer. Measuring conditions for  $T_{cp}$  determination can be in the range of 5–10 mg mL<sup>-1</sup> for concentration, 0.5–1.0 °C min<sup>-1</sup> for heating rate at a wavelength of incident light between 500–700 nm.<sup>47</sup> The turbidimetry measurement is generally performed in dilute concentration. Georgiou and co-workers studied the cloud points of 1% w/w EG-based homopolymers with different molecular masses and the number of EG units in deionized water, phosphate-buffered saline solution, and a water/ethanol mixture. They concluded that the cloud points of these homopolymers decreased as the number of EG units

decreased or the molecular masses increased. Also, they reported a significant effect of the end group of the side chain on the cloud points.<sup>292</sup> Another way to observe and quantify the thermoresponsive behaviors of polymers is to use fluorescent dyes and fluorescence spectroscopy.<sup>97,254–256</sup> Zhang *et al.* applied fluorescence spectroscopy to investigate the thermoresponsivity of copolymers of OEGMA and poly(D-lactic acid) (PDLA) and copolymers of OEGMA and PLLA.<sup>151</sup> They showed that the fluorescence intensity ratio decreased as temperature increased because of the aggregation-induced quenching of the fluorescence. By measuring the fluorescence or absorbance of the solutions, Liu *et al.* were able to investigate the thermally induced aggregation processes of their OEG-based dendronized copolymers.<sup>255</sup>

**4.1.3. Light scattering measurements.** Dynamic light scattering (DLS) provides information about the size and size distribution of polymer particles in solution as a function of temperature. DLS gives insight into the phase behavior, structural changes of the polymer, and the transitions that occur as the temperature is changed. The size determination by DLS measurement is strongly dependent on the concentration and heating rate. The intensity of the scattered light, proportional to the diameter of a particle or aggregates, dramatically increases during the coil-to-globule transition. Besides working as a basic tool to measure the size distribution of polymeric micelles and aggregates, DLS can be used to determine the LCST value<sup>257,258</sup> and  $T_{cp}$  (Fig. 11B).<sup>252,259–262</sup> When using DLS,  $T_{cp}$  is the temperature at which a sudden change in particle size occurs.<sup>182,263</sup> Fig. 12 shows a change in a particle size distribution of a thermoresponsive dendronized polymer as a function of temperature.<sup>269</sup> Overall, DLS can provide more accurate  $T_{cp}$  of thermoresponsive polymers in physiologically relevant solutions for biomedical applications and can allow more sensitive determination of large aggregates, hence the onset of the phase transition even before the formation of a cloudy solution.<sup>264</sup>



**Fig. 11** (A) Transmittance as a function of temperature measured by turbidimetry (solid line, heating; dotted line, cooling) and (B) hydrodynamic radius ( $R_h$ ) as a function of temperature recorded by dynamic light scattering for an aqueous solution of a copolymer poly(MEO<sub>2</sub>MA-co-OEGMA) (full symbols, heating; empty symbols, cooling; full line, a Boltzmann fit). Reprinted with permission from ref. 106. Copyright 2007, American Chemical Society.





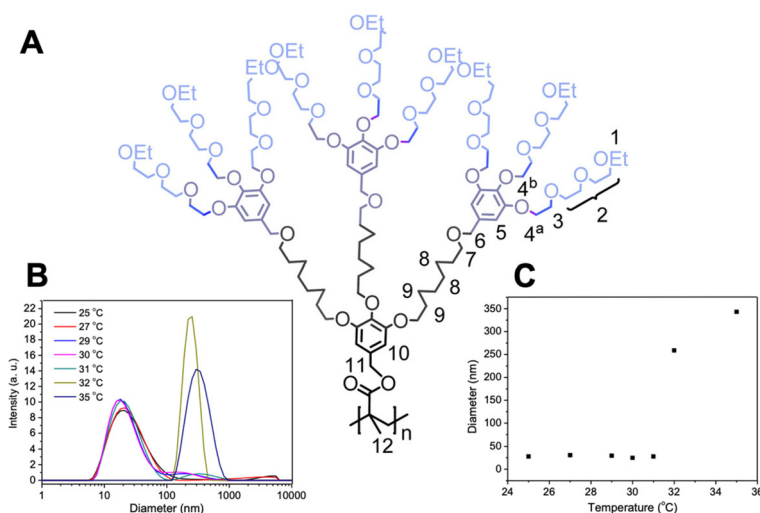


**Fig. 12** (A) Chemical structure of a thermoresponsive dendronized polymer. Dynamic light scattering measurements at different temperatures: (B) particle size distribution at different temperatures and (C) hydrodynamic diameter vs. temperature. Adapted with permission from ref. 269. Copyright 2016, American Chemical Society.

**4.1.4. Small-angle scattering techniques.** Small-angle scattering techniques allow analysis of structural changes in polymers, surfactants, colloids, proteins, and porous material in response to external stimuli. Small-angle scattering of X-rays (SAXS) and neutrons (SANS) is a fundamental measurement tool for the analysis of thermoresponsive polymers and can be performed in a dilute aqueous solution at different temperatures.<sup>266,293</sup> For SAXS analysis, a highly collimated monochromatic X-ray beam is transmitted through a sample, and the scattered X-rays are then collected by a detector at a continuous range of scattering angles. By doing so, SAXS not only is able to determine the shape and organization of large molecules but can also quantitatively characterize the conformational dispersity. The morphology determined by SAXS is of great relevance, especially regarding micelles, in which an observable response is present with a change in external stimuli, especially temperature when dealing with thermoresponsive polymers. Precise control of the structure of micelles is essential in the development of stimuli-responsive micelles that can be applied in the biomedical field for drug delivery and diffusion. Chang *et al.* examined the effect of stereocomplex crystallization on micelles, utilizing SAXS to determine the exact micelle structure as well as the thermally induced structural changes of the micelles when the temperature was raised.<sup>254</sup> Based on the SAXS, it was determined that the stereocomplex led to structural changes resulting in larger micelles with higher aggregation, this aggregation facilitated intermicellar aggregation upon heating and was responsible for the resulting thermoresponsive behavior at higher temperatures. This was due to stronger intermicellar attraction caused by structural changes upon heating. The mechanism, otherwise known as crystallization-tuned thermoresponsivity, demonstrated that structural changes (*i.e.*, crystallization) can induce phase transitions. It also proved that it is possible to

control the structural changes induced by varying temperatures, which can be utilized to design responsive micelles effectively and efficiently. Read *et al.* further expanded on the idea of using SAXS to identify the structural changes associated with the formation of aggregates with changing temperature; however, the focus is on the formation of polyion complexes comprising thermoresponsive polymers as opposed to stereocomplex.<sup>265</sup> SAXS analysis determined the large size of block polymers to be consistent with the formation of large micelles. Additionally, polyion complexes were still present at increased temperatures, but in the study conducted by Chang *et al.*, structural changes were observed and impacted aggregation behavior. Thermoresponsive polymers have also been known to be stimulus-responsive to water, another external stimulus whose observable change in morphology can be detected by SAXS. Lyngsø *et al.* utilized SAXS to gain insight into stimuli-responsive star PNIPAM polymer in water and its varying arm configurations and size.<sup>266</sup> The SAXS analysis showed some variations for individual stars, likely attributed to the differing dispersity between stars. Yet, it could not be concluded that a change in morphology directly corresponds to a change in the number of arms since it is invariably linked to a change in molecular mass. On the other hand, SAXS can provide information on phase transitions of thermoresponsive polymers. Korpanty *et al.* applied SAXS to understand the thermal morphological transitions of PDEGMA-based block copolymers.<sup>267</sup> The results indicate a potential mechanism for triblock thermal transformation, emphasizing the potential of SAXS to advance our understanding of complex nanoparticles.

In SANS experiments, neutrons penetrate into samples and scatter from the nuclei as a function of angle. The SANS technique can be used to analyze individual polymer chain conformation in a dilute aqueous solution of thermoresponsive polymers. SANS is a more suitable technique for low electron



density polymers than SAXS since the difference in neutron scattering lengths between two different nuclei (*e.g.*, hydrogen and deuterium) is large and detectable and SAXS is only sensitive to electron density rather than the nuclei.<sup>294</sup> The growth and morphology of microgel P(MEO<sub>2</sub>MA-*co*-OEGMA<sub>500</sub>) particles were previously investigated by using SANS.<sup>295</sup> Nishi *et al.* performed SANS measurements to understand the tacticity effect on phase separation for PNIPAM aqueous solution. The results revealed that hydrophobicity of PNIPAM containing *meso*- and *racemo*-isomers increased with increasing the *meso*-content.<sup>296</sup> SANS and DLS were used to study the aggregate behavior of thermoresponsive triblock PSt-PNIPAM-PSt copolymer in water as a function of temperature. The SANS and DLS measurements showed that the triblock copolymer underwent first shrinking close to the LCST and further clustering above the LCST.<sup>297</sup> Papadakis and their team used thermoresponsive poly(2-oxazoline) gradient copolymers and showed the collapse of small aggregates right above the cloud point and the formation of larger aggregates at higher temperatures by utilizing time-resolved SANS experiments.<sup>298,299</sup> SANS was also used to investigate changes in the nanostructure of double network thermoresponsive hydrogels induced by temperature change. The double network hydrogels were prepared from densely crosslinked PNIPAM first network and loosely crosslinked hydrophilic polyacrylamide second network. The SANS intensities from the double network were reported lower than those from PNIPAM single network. Lower scattering was attributed to increased water content in the double network due to the presence of the hydrophilic second network.<sup>300</sup> Overall, small-angle scattering techniques have become a powerful tool for the structural analysis of thermoresponsive polymers in physiological conditions. However, these techniques present several challenges including high-quality sample preparation and data interpretation and more importantly the cost of the analysis. Although the applicability of these techniques spans across disciplines, the availability of the instruments may be limited to the national labs or shared instrument facilities.

**4.1.5. NMR for diffusion coefficient measurements.** <sup>1</sup>H NMR spectroscopy of thermoresponsive polymer solutions can be performed at different temperatures to show the insolubility of the polymers above LCST from peak suppression.<sup>301,302</sup> In order to measure the change in the size of polymers as a function of temperature, a temperature-controlled diffusion-ordered NMR spectroscopy (DOSY) experiment can be performed. The diffusion coefficient (*D*) gives the mobility of a certain species, dependent on both their size and shape. The diffusion coefficient allows one to determine the rate at which a molecule will diffuse across a solution. Typically, molecules and polymers in smaller sizes have a greater diffusion coefficient. However, there are cases in which thermoresponsive polymers with similar molecular masses have different diffusion coefficients. This is likely attributed to differing spatial arrangements (*i.e.*, the packing arrangements of groups within the polymers). Dense packing can be regarded as a form of “shrinkage”, although not uniformly distributed nor identical in different molecules of the same polymer, thus

indicating a greater diffusion coefficient and smaller polymer size in solution. This was observed in a study conducted by Wang *et al.*, in which two thermoresponsive hyperbranched polymers based on the poly(ethylene imine)s (HPEI) skeleton were synthesized. Two spatial isomers with two kinds of amide units (*i.e.*, acetamide on C2, and isobutyramide on C4) were located on the different layers of the globular HPEI macromolecules. The polymers labeled as HPEI-C4-C2 and HPEI-C2-C4 were expected to have similar molecular size and dispersity due to almost identical chemical composition.<sup>268</sup> Yet, HPEI-C4-C2 had a higher diffusion coefficient than HPEI-C2-C4, and thus a smaller size attributed to a densely packed arrangement.

The size of thermoresponsive polymers can be further determined as the diffusion coefficient can be expressed as a function of viscosity and temperature in regard to the Stokes–Einstein equation:  $D = kT/6\pi\eta R_H$  (where *k* is the Boltzmann constant, *T* is temperature,  $\eta$  is the viscosity of the solution, and *R<sub>H</sub>* is the radius of the solvated species).<sup>229</sup> As temperature increases, polymers will have coil-globule structural changes and the size of the aggregates will change. This relationship is illustrated through the DOSY experiment in which peaks in NMR spectra of different compounds are separated based on varying diffusion coefficients and therefore differences in viscosity and temperature. DOSY can also measure molecular translational diffusion coefficients and particle size distributions, and because aggregates result in different diffusion coefficients, DOSY can determine how many aggregates with different sizes are formed. Additionally, DOSY can determine the number of aggregated species that are formed in connection with thermoresponsive globular structure formation in the solution.

The diffusion coefficients determined by DOSY can be used to derive the hydrodynamic radius of the polymers for determining size distribution and aggregation. In an aggregation study utilizing DOSY conducted by Zhang *et al.*, DOSY spectra of dendronized polymers displayed similar diffusion coefficients below the LCST (25 °C) but different diffusion coefficients above the LCST (32 °C).<sup>269</sup> It was concluded that above the LCST, OEG chains likely aggregate from the same and adjacent dendron units, resulting in a larger molecule, as supported by smaller diffusion coefficients. It is possible that the OEG chains also nonuniformly aggregate from peripheral dendrons, hence differences in diffusion coefficients and molecular size are observed. Other 1D and 2D NMR techniques can also be utilized to monitor the aggregation process and phase transition of thermoresponsive polymers.<sup>303,304</sup>

## 4.2. Bulk characterization

**4.2.1. Thermal analysis.** Typical characterization methods for thermal analysis of any polymers include differential scanning calorimetry (DSC) and thermogravimetric analysis (TGA). DSC alone cannot directly determine the LCST of a thermoresponsive polymer but DSC is important to study thermoresponsive polymers since it provides valuable information including thermal transitions<sup>275,276</sup> as well as glass transition temperature (*T<sub>g</sub>*)<sup>241,277–279</sup> and the crystallization behavior of



the polymer. The  $T_g$  provides insights into the polymer's segmental mobility and its potential thermoresponsivity. DSC can also identify the presence of crystalline domains in semi-crystalline polymers and determine their melting temperature. This information is crucial for understanding the polymer's behavior at elevated temperatures. Moreover, DSC can measure the heat flow associated with thermal transitions, providing information about the enthalpy changes that occur during these transitions. The heat capacity changes can offer insights into the polymer's interactions with the surrounding environment and help characterize its response to temperature variations. While DSC does not directly determine the LCST, it can be used in combination with other techniques, such as turbidity measurements, spectroscopy, or rheology, to investigate the LCST behavior of thermoresponsive polymers. DSC can be applied to determine the grafting ratio combined with FTIR spectroscopy<sup>229</sup> and to study the hydration/dehydration process of polymer segments.<sup>252,280,281</sup> TGA provides information about the thermal stability and degradation behavior of thermoresponsive polymers.<sup>282,283</sup> TGA can be used to identify the temperature at which the polymer begins to decompose and the rate of decomposition. TGA can also be used to determine the amount of residual solvent or other volatile impurities in the polymer, which can have a significant impact on its thermal behavior and performance.

**4.2.2. Contact angle measurements and ellipsometry.** To study the surface properties of thermoresponsive polymers, contact angle measurements and ellipsometry have been used for thermoresponsive “smart” surfaces. Contact angle measurement is a method used to determine the wetting properties of a solid surface by a liquid droplet, typically water. The LCST behavior of thermoresponsive polymers is influenced by the interaction between the polymer and water molecules. When a thermoresponsive polymer is more hydrophilic below its LCST, it is highly wettable by water, and the contact angle between the polymer surface and water droplet is small. However, when the temperature of the system is raised above the LCST, the polymer undergoes a phase transition to a hydrophobic state, which leads to an increase in the contact angle between the polymer surface and water. By measuring equilibrium water contact angles in the captive bubble configuration of the bulk of the PMEO<sub>2</sub>MA brush, Laloyaux *et al.* were able to observe the sharp variation of surface properties.<sup>270</sup> Their observations supported theoretical predictions about the vertical phase separation during the collapse. In a different work, Li *et al.* used water contact angle to characterize the surface wettability of their PNIPAM gradients.<sup>271</sup> Ellipsometry is a sensitive and non-destructive optical measurement technique to analyze the changes in the refractive index and thickness of thin films and surfaces. Below the LCST, the polymer is in a hydrophilic state, and the polymer-water interaction is strong. This interaction leads to the formation of a highly hydrated layer on the surface of the polymer, which increases the effective thickness of the polymer film. Above the LCST, the polymer becomes more hydrophobic and the interaction between the polymer and

water molecules weakens, resulting in the collapse of the hydrated layer and a decrease in the effective thickness of the polymer film (Fig. 13). Robertson *et al.* applied ellipsometry to study the overall thermoresponsive behavior of POEGMA brushes in aqueous mixed electrolytes.<sup>273</sup> Schmaljohann *et al.* studied the patterned hydrogel of PNIPAM-*g*-PEG by using imaging ellipsometry.<sup>274</sup> They were able to identify the regions of interest on a micrometer level and monitor the swelling of the hydrogel as a function of the temperature.

**4.2.3. Atomic force microscopy (AFM).** AFM is a surface analysis technique primarily used to image and manipulate atoms and structures on surfaces as well as localize different forces, such as adhesion strength, magnetic forces, and mechanical properties. There are two main modes: contact and tapping. Both can be utilized for imaging and topographic information by scanning the surface with a cantilever. The physical patterns and topography determined by AFM are of great relevance for thermoresponsive polymers and biotechnological applications, as elastic properties and surface charges influence cell culture, adhesion, and growth. Cell culture response was evaluated how the physical and chemical properties were affected by the thermoresponsive behaviors of poly(NIPAM-*co*-acrylamidebenzophenone) (AcBzPh) and poly(NIPAM-*co*-AcBzPh-*co*-*N*-*tert*-butylacrylamide) through AFM analysis by Healy and co-workers.<sup>286</sup> AFM thickness and roughness film analysis confirmed the disparity in roughness and thickness of physically adsorbed thermoresponsive films due to the adsorbed temperature conditions. Teunissen *et al.* demonstrated the reversible thermoresponsive behavior of pyrrolidone-based brushes using phase-controlled AFM topography measurements in an aqueous environment.<sup>201</sup> Polymer brush thickness was reduced by *ca.* 25% upon the expulsion of water above the LCST as compared to previous reports on PNIPAM (~20%) and poly(MEO<sub>2</sub>MA-*co*-OEGMA) (~16%) (Fig. 13).<sup>245,305</sup> Forg *et al.* further studied the adhesion properties, specifically those of PNIPAM microgels with dopamine methacrylamide, utilizing AFM to determine if the microgel particles adsorbed on a silicon wafer as well as if adhesion rates increased with the incorporation of dopamine methacrylamide.<sup>76</sup> According to the AFM results, the incorporation of dopamine methacrylamide not only increases the adsorption



**Fig. 13** Schematic illustration of the conformational change of a polymer brush below the LCST at extended state (left) and above the LCST at collapsed state (right). Adapted with permission from ref. 201. Copyright 2022, John Wiley and Sons.



of microgels on the silicon wafers with applied mechanical stress but also exhibits enhanced adhesion. In a different study, poly[*N*-(2,2-dimethyl-1,3-dioxolane)-methyl]acrylamide (PDMDOMA) brushes were grafted from silicon wafers *via* SI-ATRP and studied through AFM force–distance measurements. PDMDOMA brushes were observed to be in a hydrated state (amphiphilic) at low temperatures below the LCST (<22–24 °C) and a dehydrated and collapsed state (hydrophobic) at high temperatures.<sup>99,306</sup> Stetsyshyn and co-workers studied wetting, morphology, and protein adsorption of thermoresponsive P(4VP-*co*-OEGMA<sub>246</sub>) polymers and demonstrated changes in surface roughness and adsorption behavior induced by two-stage temperature transitions using AFM. The surface topography of copolymer and homopolymers at three different temperatures was examined in noncontact mode and characterized by root-mean-square (RMS) values. The roughness increased for homopolymers as the temperature rose from 10 °C to 30 °C. In contrast, the copolymer showed temperature-controlled switching of morphology (Fig. 14).<sup>307</sup>

AFM is also used to determine the topological effects on thermoresponsive behavior. Changes in structures, number of arms, and crosslinking can alter the thermoresponsiveness of polymers as it affects phase transitions. Phase transitions from a rigid to a flowing state or *vice versa* can alter how cells interact with each other and on surfaces. More specifically, Oleszko *et al.* utilized AFM to determine how poly(2-isopropyl-2-oxazoline) (PIPOx) surface crystallinity on a thermoresponsive influence on cell adhesion and detachment.<sup>285</sup> AFM analysis detected thermoresponsive-induced changes in physico-chemical properties, such as the formation of PIPOx crystallites, that promote cell adhesion and cell detachment.

Regarding AFM's ability to detect topography, Tao *et al.* observed the thermoresponsive properties of dendritic macromonomers and dendronized polymers through the examination of topology with AFM.<sup>101</sup> AFM measurements verified a mixture of bulk polymers. Additionally, it was found that the fan-shaped topology of the dendritic macromonomers changes to cylindrical for dendronized polymers, having significant effects on the thermoresponsive behavior. Similarly, Arias *et al.* observed the chiro-thermoresponsive (*i.e.*, thermoresponsive behavior through conformational changes) properties of helical poly(phenylacetylene) bearing elastin-based side chain polymers.<sup>281</sup> The AFM revealed a spherical morphology of the polymers, an unexpected thermoresponsive conformational change on the synthesized helical side chains of the elastin polymers. This is suggesting that the helical structure is of great importance in thermoresponsive behavior.

**4.2.4. Electron microscopy.** Scanning Electron Microscopy (SEM) can give information about the surface morphology and topography of thermoresponsive polymers. In SEM, a focused beam of electrons is scanned over the surface of the material, generating signals that are used to create an image of the surface. SEM can provide high-resolution imaging with a large depth of field, allowing researchers to visualize the three-dimensional surface features of the material. This can be particularly useful for understanding how temperature changes affect the surface morphology of thermoresponsive polymers, such as the formation of surface domains, changes in roughness, and the emergence of new surface features. Additionally, SEM can also be used to study the thermal stability of thermoresponsive polymers by monitoring changes in the surface morphology during heating or cooling. SEM images can help

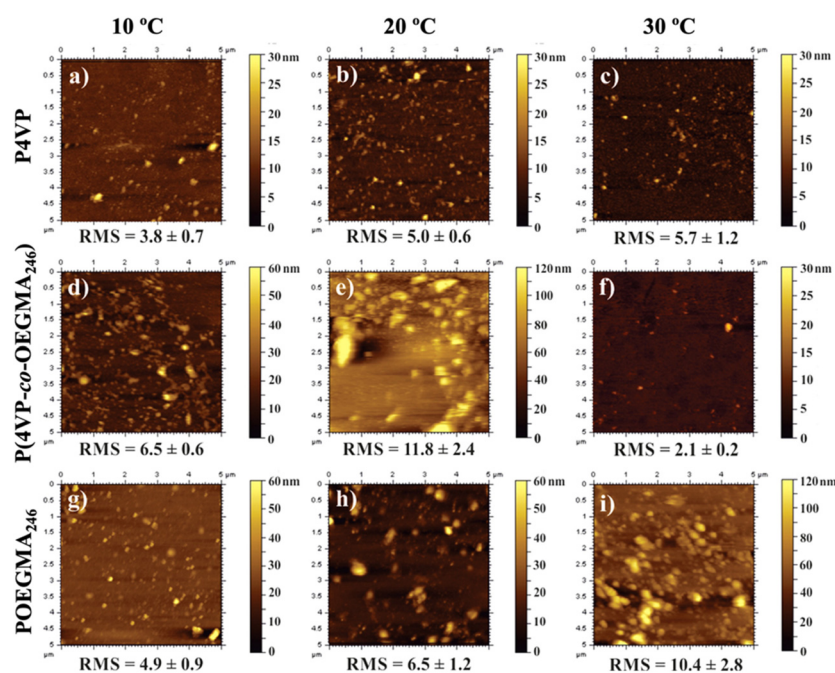


**Fig. 14** AFM topography of P4VP (a–c), P(4VP-*co*-OEGMA<sub>246</sub>) (d–f), and P(OEGMA<sub>246</sub>) (g–i) grafted brushes at different temperatures. Adapted with permission from ref. 307. Copyright 2017, American Chemical Society.





quantify changes in surface roughness, the formation of new surface features, and any morphological changes that occur during temperature changes. Transmission Electron Microscopy (TEM) provides high-resolution imaging of the internal microstructure of thermoresponsive polymers. By using TEM, the microstructure can be visualized at different temperatures, and changes in their physical properties can be related. TEM imaging can also be used to study the size and distribution of polymer chains, as well as any aggregates or phase separations that may occur (Fig. 15). These observations can then be related to the temperature-responsive behavior of the material, helping to gain a better understanding of its thermodynamics and thermophysical properties. Cryogenic SEM/TEM (Cryo-SEM/TEM) is also widely applied as a characterization method to preserve the native state of the sample and avoid sample degradation. Nguyen *et al.* used cryo-SEM to analyze their freeze-dried samples of PNIPAM-based polymers.<sup>229</sup> They found out that for polymers with similar chemical composition, more branching enables access to hydrogels with smaller pore sizes. A good correlation between the decrease of  $G'$  modulus and the density of entanglements between the mesoglobules was observed by Zhao *et al.* by using cryo-SEM.<sup>252</sup> Cryo-TEM imaging can shed light on the hydration process, pore sizes, and structural changes upon cooling and warming up.<sup>284</sup> Korpanty, Gianneschi, and co-workers used variable temperature liquid-phase TEM of PDEGMA triblock system to observe the formation of intermediate structures during the morphological transformation of the polymer in response to variations in temperature.<sup>267</sup>

**4.2.5. X-ray photoelectron spectroscopy (XPS).** XPS is a technique mostly used in surface chemistry. Through depth profiling, XPS utilizes an ion beam to methodically remove the outermost 30 atomic layers (approximately 10 nm), retrieving

data on each layer and creating a high-depth composition profile. This profile allows for determining the composition of surface material elements, their relative abundance, as well as the chemical state of the polyvalent ions. Surface material elements in thermoresponsive polymers can result in surface wettability and adhesive characteristics and fluorophores can also be tethered to produce fluorescent characteristics. XPS is essential in biomedical applications to confirm successful surface modification. Teunissen *et al.* utilized XPS to determine if the synthesis of thermoresponsive poly(*N*-(2-methacryloyloxyethyl)pyrrolidone (poly(NMEP)) brushes was successful, as the synthesis aimed to combine a more controlled polymerization with thermoresponsive behavior.<sup>201</sup> The XPS spectra confirmed the synthesis of these poly(NMEP) brushes due to the nitrogen present in the monomer's pyrrolidone ring, resulting in a supporting signal appearance at 400.0 eV. This confirmed poly(NMEP)'s thermoresponsive behavior and demonstrated the possibility of it as a smart coating in biomedical devices. Li *et al.* synthesized silver nanoparticles (AgNPs) as cores and fluorophore-tethered thermoresponsive copolymers, oligo(ethylene oxide) acrylate, and di(ethylene oxide) ethyl ether acrylate, as shells to produce a metal-enhanced fluorescence effect, utilizing XPS to confirm the success of the synthesis.<sup>256</sup> The XPS spectra showed the presence of copolymer on the surface of the AgNPs, indicating the successful preparation of the AgNP/polymer nanohybrids.

XPS is not limited to biomedical applications, but also to the biocompatibility of polymers, as surface adhesion is also of importance in cell cultures. By determining the composition of the surface layers, conclusions can be made on cell adhesion and attachment. Cell adhesion is fundamental in cell communication, regulation, maintenance, and growth, whereas cell detachment is essential in culturing cells. Thermoresponsive polymers can be used as a non-invasive control for adhesion and detachment by altering the temperature. Two studies examined the characteristics of thermoresponsive polymer layers used in the development of cell cultures. Oleszko *et al.* focused on thermoresponsive PIPOx layers, as these layers are used as biomaterials for human dermal fibroblast culture and detachment.<sup>285</sup> The surface composition was determined through XPS, revealing the contents of carbon and nitrogen atoms. Therefore, the high crystallite content of PIPOx promoted the adhesion of the fibroblasts. PNIPAM has also been regarded for cell culture. Its chemical composition was analyzed through XPS in a study by Healy and co-workers, with the goal to make cell sheet regeneration more feasible and accessible.<sup>286</sup> It was concluded that thermoresponsive film based on PNIPAM supports cell adhesion and temperature-controlled cell sheet detachment. The results demonstrated that thermoresponsive films successfully promoted cell adhesion and temperature-controlled cell detachment. This is beneficial as thermoresponsive surfaces can detach confluent cell sheets in a less invasive manner, allowing the detached sheets to be transplanted for further *in vitro* and *in vivo* adhesion and applications.



**Fig. 15** TEM micrographs (left) and DLS particle size distribution by intensity (right) of micelles in copolymer solution. Reprinted with permission from ref. 289. Copyright 2012, American Chemical Society.



**4.2.6. X-ray powder diffraction (XRD).** XRD, a bulk technique often correlated with microscopy, is based on constructive interference of monochromatic X-rays and crystalline samples. The resulting data can confirm phase identification of crystalline matter as well as unit cell dimensions; in the case of polymeric materials, XRD is often utilized to determine the degree of crystallinity and phase ratio. More specifically, thermoresponsive polymers can experience a change in the degree of crystallinity and dimensions initiated by temperature change. Kumar *et al.* utilized XRD analysis of poly(NIPAM-*b*-DMA) thermoresponsive diblock copolymer grafted onto  $\beta$ -cyclodextrin to determine crystalline alterations.<sup>283</sup> The XRD pattern confirmed PNIPAM was well connected in the diblock copolymer and  $\beta$ -cyclodextrin frame. Similarly, Jadhav *et al.* used XRD analysis on PNIPAM, specifically with post-synthesis grafting as opposed to star polymers, to determine the thermal stability and pore uniformity.<sup>287</sup> The XRD spectra illustrated a high degree of structural order with pores in a hexagonal setting. Of great importance, XRD demonstrated that the characteristic-ordered mesoporous structure remained intact throughout the polymerization, proving that the grafted polymer could maintain its characteristic mesoporous structure while exhibiting thermoresponsive behavior.

## 5. Biomedical applications of thermoresponsive polymers

Advancements in thermoresponsive materials have had a profound influence on numerous biomedical domains. The distinctive characteristic of reversible phase transition, occurring near physiological temperatures and allowing thermogelation for local treatment or use in wound healing, positions these materials as highly promising for an extensive range of biomedical applications. Such applications encompass bioimaging, biosensing, drug delivery systems, injectables, smart surfaces, bioadhesion, biomanufacturing, and tissue engineering.

### 5.1. Bioimaging and biosensing

Thermoresponsive polymers can be functionalized with different types of contrast agents or biomolecular probes for imaging and sensing applications. These materials can be chemically tuned to enable temperature-dependent phase transitions to respond to disease biomarkers, such as in cancer diagnostics, and in general assist in the monitoring of disease progression and drug delivery efficiency.<sup>308–312</sup> The unique properties of thermoresponsive polymers to undergo sol-gel transition above a certain temperature makes them promising materials for local delivery and long-term monitoring of therapeutic and diagnostic (theranostic) agents. For example, Kim *et al.* developed a poly(organophosphazene)-based hydrogel system that contained magnetic nanoparticles for long-term magnetic resonance (MR) imaging and cancer drug delivery application. Using their thermosensitive hydrogel system they were able to demonstrate the *in vivo* efficacy of long-term MR

theranostics over a period of three weeks using their tumor-bearing mice model.<sup>308</sup> In another study conducted by Wang *et al.*, they used a PNIPAM-coated multifunctional nanoparticle system for combined fluorescence and MR imaging to track transfused cells *in vivo*. This new modality of cell tracking can be used for monitoring cell therapeutics such as in stem cell transfusion to cure leukaemia and other diseases.<sup>309</sup>

In addition, thermoresponsive polymers have been exploited for applications in biosensing and can be utilized to detect various biological signals, such as changes in pH, temperature, and the presence of specific biomarkers or pathogens. Antunez *et al.* synthesized a thermoreversible biosensor for detecting heat-labile enterotoxin from the pathogen *Escherichia coli* which is known to cause diarrhea. The biosensing platform is composed of a porous silicon interferometric transducer and a thermoresponsive multivalent glycopolymer receptor that allows the reuse of the biosensor and subsequent detection cycles.<sup>310</sup> In another study, Elshaarani *et al.* developed a glucose sensor based on 3-acrylamidophenylboronic acid and PNIPAM. Moreover, this sensor can detect different concentrations of glucose as glucose accumulates on the hydrophilic PNIPAM chains through hydrogen bonding, and as the temperature increases above 25 °C the hydrogel shrinks due to the thermoresponsive nature of the PNIPAM chain. This phenomenon in turn limits the accessibility of the phenylboronic acid component for glucose complexation as its conformation changes from coil to globule shape.<sup>311</sup>

Fluorescent dyes can also be incorporated into the polymers for development of biosensors. Mao *et al.* utilized OEGylated cyclodextrin-based thermoresponsive polymers as switchable inclusion complexes for fluorescent dyes. The OEG units work cooperatively towards the formation of inclusion complexes with fluorescent dyes that leads to significant changes in the monitored optical response of the system. The encapsulated dyes can be released upon heating, resulting in a noticeable decrease in fluorescence *via* quenching. This makes cyclodextrin polymers suitable for use as the foundation for temperature-responsive fluorescent sensors.<sup>312</sup> Overall, the temperature sensitivity of thermoresponsive polymers makes them useful tools in biosensing, allowing for the detection of various biological signals in real-time and providing new methods for monitoring biological processes.

### 5.2. Therapeutics

**5.2.1. Drug delivery systems.** Extensive research has been conducted on responsive drug delivery systems for controlled and sustained drug release on targeted sites.<sup>313–316</sup> This facilitated a closer study of polymers which have properties that can be controlled by external stimuli such as electricity, ultrasound, oscillating magnetic fields, enzymes, pH change, light, and thermal energy.<sup>250,317</sup> Of particular interest are thermal-responsive polymers, which allow for the control of physical properties by changes in the temperature of the environment. For example, below the LCST, PNIPAM is hydrophilic and water-soluble or swells in gel systems. Above the LCST, PNIPAM diblock copolymer drug delivery system undergoes a



“coil-to-globule” reversible phase transition that leads to a dramatic shrinkage in volume (Fig. 16).<sup>318,319</sup>

In the past, many PNIPAM-based delivery systems have been engineered. Nayak *et al.* successfully synthesized a structurally hollow PNIPAM gel from core-shell nanoparticles. These hollow structures show higher equilibrium swelling volumes below LCST and a greater deswelling ratio above LCST.<sup>318</sup> Aside from thermal control, the drug delivery systems must be stable at physiological pH, but to enable degradation for clearance should hydrolyze in a slightly acidic environment. To accelerate the hydrolysis reaction the polymer side changes were modified with additional hydroxyl groups.<sup>320</sup> Thermoresponsive delivery systems are highly desirable for cancer treatment as they show strong enhanced permeation and retention effect in targeting cytotoxic drugs to solid tumor tissues.<sup>280,321</sup> An example of a cancer drug that exhibits adverse side effects is doxorubicin. Using a star-block poly( $\epsilon$ -caprolactone)-*block*-PME<sub>2</sub>OMA-*co*-POEGMA that self-assembles into a micelle, Li *et al.* were able to show low cytotoxic delivery of doxorubicin that also was effective in inhibiting HepG2 cell proliferation.<sup>54</sup> Another promising delivery system for doxorubicin is thermogelling glycol chitin, which displayed easy encapsulation and sustained drug release over a 13-day period.<sup>322</sup> Paclitex is a natural anticancer drug containing Cremophor EL (polyoxyethylated castor oil) that also has many side effects including bronchospasm, hypotension, and hypersensitivity. Paclitex also faces multi-drug resistance from cancer cells and has poor water solubility. These challenges restrict the drug's dosage and infusion period. Song *et al.* demonstrated that by using a thermoresponsive polymer system consisting of a  $\beta$ -cyclodextrin as a core to a four-armed PNIPAM to encapsulate Paclitex, the cellular uptake of the drug can be enhanced, and multidrug resistance can be overcome making the polymer an ideal candidate for cancer therapeutics.<sup>144</sup> A very few of these thermoresponsive micellar drug delivery systems have been tested for the later stages of clinical trials. One PEG-poly(D,L-lactide) system under the name of Genexol-PM has received approval for breast and lung cancer

treatments.<sup>323</sup> There are other several PEG-based micellar systems currently under Phase I–III clinical trials.<sup>14</sup>

In addition to cancer therapy, ocular diseases are promising targets for thermoresponsive therapeutic systems.<sup>324</sup> Eye diseases are generally treated by the ocular installation of drugs as it is a non-invasive route and allows for easy administration. However, only about 5% of the administered drug infiltrates the cornea to the intraocular tissue through conventional eye drop formulations as such improving the bioavailability and targeted delivery of ocular drugs remains a challenge. By taking advantage of the interactions of cyclodextrins with hydrophobically modified polymers, Iohara *et al.* prepared a thermoresponsive hydrogel system for ocular applications. By adding  $\alpha$ -cyclodextrin to hydrophobically modified hydroxypropyl methylcellulose, the resulting cellulose/cyclodextrin gel could undergo a reversible sol-gel transition under physiological temperature, and they demonstrated the effective delivery of diclofenac sodium in the eyes of a rabbit animal model. Moreover, the cyclodextrin improved the drug's bioavailability and bioabsorption.<sup>52</sup>

**5.2.2. Injectables.** Certain thermoresponsive polymers have been utilized as injectables for treating biofilm-related infections, such as prosthetic joint infections, because of their potential low toxicity, biocompatibility, and biodegradability.<sup>325–327</sup> Glycol chitin, a water-soluble thermoresponsive polymer derived from glycol chitosan, can transition from a liquid to a gel state at varying temperatures by adjusting the level of *N*-acetylation and the concentration of the polymer in the solvent used for delivery.<sup>322</sup> The formation of a gel in chitosan-based hydrogels occurs due to hydrophobic and hydrogen bonding interactions between the polymer chains. As the gelation process results from these weak interactions, it can be reversed.<sup>328</sup> Milbrandt *et al.* have utilized a treatment approach that is based on a thermoresponsive glycol chitin hydrogel nanocomposite system, containing D-amino acids and light-activatable gold nanorods, which can undergo sol-to-gel transformation at physiological temperatures for site-specific eradication of mature *Staphylococcus aureus* biofilms on metal alloy implant materials (Fig. 17).<sup>327</sup> Their two-step method, which combines the use of a light-activated gold nanorods hydrogel composite system for photothermal treatment after initial biofilm disruption with D-amino acids, is bridging the gap in developing alternative therapies for prosthetic joint infections.<sup>326,327</sup>

In the case of dramatic eye injuries or diseases, rapid treatment is crucial to avoid vision deterioration. PNIPAM and its derivatives can be used as a bioadhesive for treating ocular complications.<sup>329–331</sup> As a substitute for sutures or cyanoacrylate-based adhesive materials (*i.e.*, biomedical grade super glue), Bayat *et al.* developed a temperature-sensitive injectable hydrogel consisting of physically crosslinked PNIPAM copolymerized with *n*-butyl acrylate that functions as a temporary sealant. When tested on a rabbit model with open globe injury, the hydrogel was easily applied using custom-made temperature-controlled syringes and effectively maintained intraocular pressure without causing neurotoxicity, retinal



**Fig. 16** Schematic representation of a thermoresponsive diblock copolymer drug delivery system, which contains a hydrophobic block that serves as a scaffold and an LCST block that responds to temperature changes in the environment. At higher temperatures, the LCST block shrinks and the drug is released from the system.





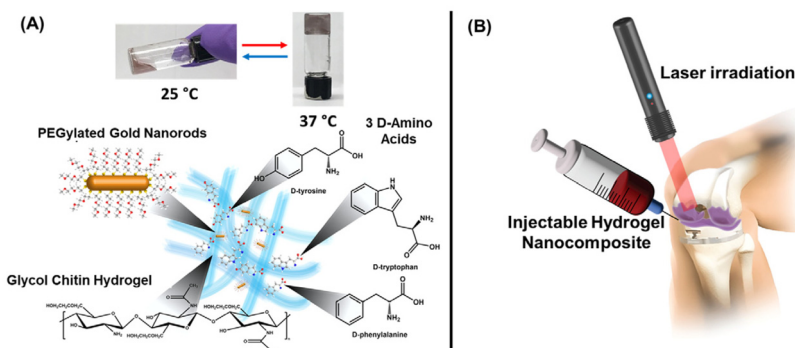


**Fig. 17** Schematic representations of the components (A) and injectable treatment approach (B) of a thermoreversible hydrogel system for the treatment of joint infections. Adapted with permission from ref. 326 and 327. Copyright 2020 and 2023, American Chemical Society.

tissue degradation, or significant chronic inflammatory response. The hydrogel can be removed by exposing it to cold water once it has set. This hydrogel can be beneficial in areas with limited resources, where it can temporarily close wounds to prevent further tissue damage or vision loss prior to surgery.<sup>330</sup> Although the mechanism was not explained, PEG-based *in situ* forming hydrogels (ReSure® sealant) were used to prevent incision leakage after cataract surgery and approved by Food and Drug Administration (FDA) and a Phase 3 clinical trial was also completed.<sup>332</sup> Fig. 18 shows PEG-PNIPAM-based thermoresponsive injectable polymers for various biomedical applications.<sup>57</sup>

Although limited, injectable thermoresponsive hydrogels have been used in clinical trials for cancer treatment. Triblock copolymers of poly(lactic-co-glycolic acid) (PLGA)–PEG–PLGA with a sol–gel transition at 37 °C commercialized under the names of ReGel® and OncoGel® were used to solubilize poorly soluble drugs and apply for local tumor management. This thermoresponsive system increased the drug loading (e.g., paclitaxel) by more than 400-fold with high drug release results and degradation over 4–6 weeks.<sup>333–335</sup> However, these

clinical trials were terminated due to lacking impact on tumor regression.<sup>336</sup> Additionally, PEG-based polymers and related technologies are the only synthetic polymeric biomaterials with a thermoresponsive transition around human body temperature approved by FDA.<sup>337</sup>

### 5.3. Smart surfaces

Thermoresponsive polymers have been quite often used as a coating material to design stimuli-responsive smart surfaces by generally chemical or sometimes physical tethering. Protocols for the production of thermoresponsive surfaces are complex, costly, and can often not yield the desired product (no control over the geometry of the surface or layer thickness). Sponchioni *et al.* developed a synthetic technique and fabricated thermoresponsive polymers enabling the coating of tissue culture polystyrene with styrene as an anchor and arginine–glycine–aspartic acid (RGD) for the collection of cell sheets in serum-free conditions. This technique required no particular equipment and allowed copolymer adsorption regardless of geometry and size.<sup>64</sup> Another approach to increasing cell adhesion is the copolymerization of dopamine

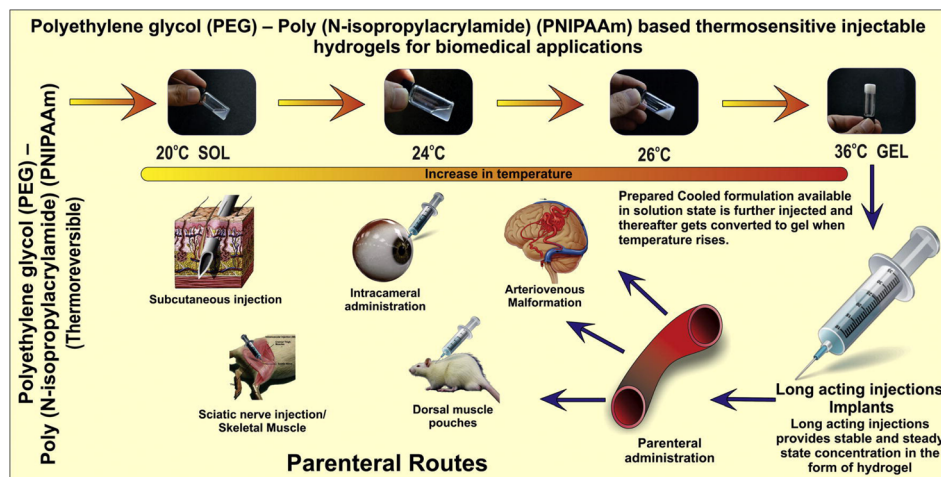


**Fig. 18** PEG–PNIPAM-based thermoresponsive injectable polymers for biomedical applications. Adapted with permission from ref. 57. Copyright 2014, Elsevier.





methacrylamide with PNIPAM. As opposed to pure PNIPAM microgels, the resulting P(NIPAM-co-dopamine methacrylamide) microgel exhibited enhanced adhesion even under harsh conditions (*i.e.*, mechanical stress).<sup>76</sup> It is important to note that the nature and concentration of the ion strongly influence the thermoresponsive properties of polymeric gels and brushes.<sup>250</sup>

Polymeric hydrogels are often modified with amino acid sequences like RGD to increase their cell adhesion properties.<sup>74,338</sup> Marrow stromal cells were used to test the adhesive properties of these RGD-modified hydrogels. After 28 days, adhesion of the cells was observed as well as successful proliferation.<sup>338</sup> Additionally, the copolymerization of insulin and RGDS (arginine-glycine-aspartic acid-serine) demonstrated site-selective cell adhesion and growth along with the temperature-dependent spatiotemporal detachment of sparsely adherent and confluent cells. From a peptide-based approach, RGDS and insulin were immobilized onto thermoresponsive surfaces for site-selective cell adhesion and growth, which allowed for site-specific harvest. Moreover, selective recovery of either contiguous monolayer or mesh-like designed monolayer tissue constructs on identical surfaces was observed.<sup>74</sup>

In addition, thermoresponsive polymers have drawn much attention in the design of smart surfaces that can be used for bioanalysis and bioseparation because of their switchable wetting properties that can be readily tuned through temperature changes in the environment. In chromatographic applications, thermoresponsive polymers can be useful in the separation of proteins and cells that can be deactivated by organic solvents that work with traditional reversed-phase chromatography column packing materials.<sup>189,339–343</sup> Kanazawa *et al.* developed an early type of thermoresponsive chromatography stationary phase made by modifying silica bead surfaces with PNIPAM *via* a coupling reaction (Fig. 19). The PNIPAM-modified silica beads were packed into a stainless-steel column and used to separate different steroids. At 5 °C all the steroids were eluted at once, but with increasing temperature the retention times were prolonged and effective separation was achieved at 35 °C and above. The effective separation could be attributed to the enhanced hydrophobic interactions between the PNIPAM-modified silica beads and the steroids at elevated temperatures.<sup>344</sup>

In biomanufacturing, microfluidic systems offer low-cost solutions for scaling up cell-based therapies to reduce health disparities. However, a major challenge is the efficient recovery of cells that are bound to microfluidic channels while maintaining their viability. Thermoresponsive polymers provide a promising approach for overcoming this limitation. By functionalizing the polymers with specific antibodies, they can be used to bind a targeted cell type for isolation, on-chip transduction, and expansion. Importantly, the temperature-triggered response of these polymers allows for the controlled release of modified cells without affecting their viability. Moreover, recent research has shown that not all CD34+ stem cells are relevant for hematopoiesis, and instead, a small subpopulation of CD34+ cells co-expressing CD90+ cells is responsible for repopulation after hematopoietic stem cell transplan-



Fig. 19 Concept of thermoresponsive bioanalysis and bioseparation using surfaces modified with thermoresponsive polymers. Reprinted with permission from ref. 342. Copyright 2016, RSC.

tation.<sup>345</sup> However, it is not currently possible to target cells that co-express multiple markers using immunomagnetic bead-based purification. To overcome this drawback, thermoresponsive polymers offer a viable platform for double positive selection, where isolated CD34+ cells can be further processed to select only cells co-expressing CD90 markers, potentially improving treatment outcomes. Gurkan *et al.* demonstrated the use of PNIPAM-coated microfluidic channels for isolation of CD4+ and CD34+ hematopoietic stem cells from unprocessed human whole blood with high specificity (90%), viability (95%), and release efficiency (60%).<sup>346,347</sup> Although selective capture of cells from bodily fluids in microchannels has been previously demonstrated by other groups, it remains a significant challenge to release the desired cells due to their strong adherence to the microchannel surface. By using thermoresponsive polymers, the same research lab was able to capture the CD4+ lymphocytes at physiological temperature and subsequently release them below the LCST (~32 °C) of the polymer.<sup>346</sup> By synthesizing a novel UV cross-linkable copolymer of 4-(*N*-cinnamoylcarbamide)methylstyrene and NIPAM, Recum *et al.* were able to develop a thermoreversible cell culture coating and grew retinal pigment epithelium cells to confluence. Then by decreasing the temperature from 37 °C to 20 °C the cells readily detach. This technology that gives rise to cell sheets without scaffolds will be useful for tissue engineering applications as it can provide cells without cell damage and serve as implanted scaffolds.<sup>348</sup>

In the case of cell transplantation to treat intractable diseases, it is crucial to develop cell separation methods whereby thermoresponsive polymers have also great potential. Recently, Nagase *et al.* synthesized a thermoresponsive cationic copoly-



mer brush (PDMAPAM-*b*-PNIPAM) that could successfully separate targeted umbilical cord-derived mesenchymal stem cells from fibroblasts and macrophages. At physiological temperature, all cell types adhere to the cationic polymer brush, however, when the temperature is reduced to 20 °C the mesenchymal stem cells detached from the polymer brush while the fibroblasts and macrophages remain adhered. As such, the prepared thermoresponsive cationic polymer brush could be used as an effective cell separation tool for the purification of mesenchymal stem cells.<sup>90</sup> By leveraging the unique properties of thermoresponsive polymers, researchers can potentially overcome some of the challenges associated with traditional cell separation techniques and develop more efficient and cost-effective methods for cell-based therapies.

#### 5.4. Tissue engineering

Due to the shortage of organ and tissue donors, much attention has been devoted to finding replacements for use in regenerative medicine and advanced tissue engineering. With cell sheet engineering, tissue-specific cells can be used for the fabrication of physically connective, functionally synchronous three-dimensional tissues.<sup>64</sup> In the case of cell-based therapies, thermoresponsive polymers serve as a good platform for scaffold-free cell growth as they permit little to no immune rejection, and display greater regenerating properties compared to directly injected suspended cells. This type of biomaterials has found applications in orthopaedic tissue engineering, wound healing, oral disease treatments, and neural and corneal tissue therapy (Fig. 20). Moreover, the ability of thermoresponsive polymers to swell in water allows for their tissue-like elastic properties and high permeability to biological fluids.<sup>349,350</sup> While designing a smart polymer material, it is important that candidate polymers are highly porous to provide cell diffusion and promotion of the developing tissues' vascularization, have easily tunable functions and properties, and be completely biodegradable. Kang *et al.* synthesized

highly porous gelatin-based scaffolds that successfully provided a way to fabricate biodegradable scaffolds with interconnective pores for mass diffusion control.<sup>349</sup> Moreover, their gelatin-based scaffolds were found to be easily integrated into human tissues.<sup>351</sup> These scaffolds can also be produced by 3D bioprinting of thermoresponsive hydrogels which has been previously reviewed.<sup>352</sup>

Macroporous constructs have become favorable materials for bone-tissue engineering as they serve as ideal scaffolds for tissue growth while allowing the use of different types of biomaterials including those that are metallic, ceramic, or synthetic polymer in nature.<sup>338,353</sup> Fu *et al.* synthesized a biodegradable triblock copolymer PEG-poly( $\epsilon$ -caprolactone)-PEG (PEG-PCL-PEG) with nanohydroxyapatite, which showed potential use in cell proliferation for bone regeneration applications.<sup>63</sup> In a similar study, Shin *et al.* were able to design a novel oligo(poly(ethylene glycol) fumarate) (OPF) hydrogel and they assessed the *in vivo* bone and soft tissue behavior in a rabbit animal model. The group was able to show the formation of a fibrous capsule around the cranial implant with a thickness that remained consistent during implantation thereby demonstrating that the OPF hydrogel invokes a tissue response. Moreover, histology revealed that OPF made from higher molecular mass PEG exhibited enhanced fragmentation and tissue infiltration by inflammatory cells making this type of material promising as a biodegradable scaffold for bone tissue engineering.<sup>350</sup>

Additionally, thermoresponsive polymers have a variety of applications in cutaneous wound healing. Injury to the skin can be treated through a multi-phase healing process involving tissue granulation and re-epithelialization. Failure in the wound-healing process can lead to chronic unhealed wounds or abnormal scarring. In a proof-of-concept experiment, Zhong *et al.* demonstrated that a citrate-based poly(poly(ethylene glycol) citrate-co-NIPAM) copolymer scaffold embedded with iKera cells provided more effective cutaneous wound healing and re-epithelialization than either the copolymer or iKera cells alone.<sup>354</sup> On a similar note, Pawar *et al.* prepared polymer blends of PNIPAM, egg albumen, and poly( $\epsilon$ -caprolactone) with the antibiotic gatifloxacin hydrochloride (Gati) to prepare nanofibers for wound healing applications. The *in vivo* studies showed faster tissue regeneration using the nanofibers which supports the suitability of Gati-loaded nanofibers for wound healing applications.<sup>355</sup> In the case of periodontal diseases, these polymers can be used to create scaffolds that mimic the natural environment of the periodontium and promote the growth of new tissue. By incorporating thermoresponsive polymers into such scaffolds, researchers can potentially create a treatment that is minimally invasive and maximally effective in treating periodontal diseases.<sup>356–359</sup> For example, Ji *et al.* developed a chitosan-based thermosensitive hydrogel made from quaternized chitosan with  $\alpha,\beta$ -glycerophosphate that they could use to promote the development of alkaline phosphatase activity in human periodontal ligament cells.<sup>356</sup>

Tissue engineering involving the neural system has generally been more challenging because of the presence of the



Fig. 20 Illustration of the different types of applications of thermoresponsive polymers in tissue engineering.



blood–brain barrier that separates the nervous system from systemic circulation and the limited self-regenerating properties of the nervous system. However, injectable hydrogels, such as 0.5% : 3% and 0.75% : 3% chitosan/ $\beta$ -glycerophosphate hydrogels developed by Bhuiyan *et al.* have been shown to have suitable properties for neural tissue engineering and supported cell growth and proliferation *in vitro*. This type of hydrogel has been demonstrated to be suitable for porosity, osmolality, and swelling behavior for neural tissue engineering and also has desirable biodegradation pathways.<sup>79</sup> Aside from neural repair applications, thermoresponsive polymers have also been demonstrated to show potential for regenerative medicine applications in the eye.<sup>360–363</sup> Khalili *et al.* were able to generate corneal endothelium-like cell sheets using alternative cells that were embedded in elastin-mimetic dendrimers.<sup>363</sup> Overall, the application of thermoresponsive polymers in tissue engineering holds great promise for developing new approaches that could be useful for regenerative medicine and pharmaceutical research.

## 6. Conclusions and future perspectives

Polymers have the ability to respond to various external stimuli such as temperature, light, and pH. Among these stimuli, thermoresponsive behavior of polymers is studied extensively. The LCST behavior of thermoresponsive polymers can be tailored through various synthetic tools including copolymerization, end-group functionalization, and modifying the architecture of the polymer. Thermoresponsive polymers with narrow molecular mass distribution, controlled molecular mass, high end-group fidelity, and various compositions and architectures can be synthesized through controlled radical polymerization techniques such as ATRP and RAFT polymerization which are ideal synthetic tools for better structural design, control, and tunability in solution and from the surface. The structural heterogeneity in polymers has a significant effect on the thermoresponsive properties. Thus, these thermal transitions should be precisely determined by using modern characterization tools such as NMR and UV-Vis spectroscopy, AFM, rheometer, and electron microscopy. The tunability of the LCST makes these polymers ideal for use in physiological temperatures. The study of thermoresponsive polymers has a broad range of current and potential future applications in drug delivery for cancer treatment, tissue engineering for regenerative medicine, injectable polymers for therapeutics, smart surface for cell separation, and several other areas. Although the earliest works on temperature-induced phase transition were reported in the late 1960s, thermoresponsive materials in the biomedical field have still been emerging and more advanced materials for use in patients can be designed by leveraging the synthetic and characterization tools highlighted in this review article.

## Abbreviations

AcBzPh	Acrylamidebenzophenone
ACPBA	Acetamidophenylboronic acid
AFM	Atomic force microscopy
AgNPs	Silver nanoparticles
ARGET	Activators regenerated by electron transfer
ATRP	Atom transfer radical polymerization
BuMA	Butyl methacrylate
CRP	Controlled radical polymerization
CTA	Chain transfer agent
DEGA	Di(ethylene glycol) monomethyl ether acrylate
DLS	Dynamic light scattering
DMA	Dimethyl acrylamide
DMAPAM	<i>N,N</i> -Dimethylaminopropyl acrylamide
DOSY	Diffusion-ordered spectroscopy
DSC	Differential scanning calorimetry
eATRP	Electrochemically-mediated atom transfer radical polymerization
EG	Ethylene glycol
eOEGMA	Ethoxy oligoethylene glycol methacrylate
FDA	Food and Drug Administration
Flu	Fluorescein
FTIR	Fourier transform infrared
HEA	2-Hydroxyethyl acrylate
HIPPVTA	Bis( <i>N</i> -hydroxyisopropyl pyrrolidone)-2-vinylterephthalate
HMS $\epsilon$ BA	Pendant disulfide functionalized <i>t</i> -butyl acrylate
HPEI	Hyperbranched poly(ethylene imine)
HPMA	<i>N</i> -(2-Hydroxypropyl) methacrylamide
LCST	Lower critical solution temperature
mDEGMA	Diethylene glycol methyl ether methacrylate
Me <sub>4</sub> Cyclam	1,4,8,11-Tetramethyl-1,4,8,11-tetraazacyclotetradecane
Me <sub>6</sub> TREN	Tris[2-(dimethylamino)ethyl]amine
MEA	Monoethanolamine
mEGA	Ethylene glycol methyl ether acrylate
ME <sub>2</sub> OMA	2-(2-Methoxyethoxy)ethyl methacrylate
<i>M<sub>n</sub></i>	Number-average molecular weight
MPEGMA	Methyl polyethylene glycol methacrylate
MR	Magnetic resonance
mTEGMA	Tetraethylene glycol methyl ether methacrylate
<i>M<sub>w</sub></i>	Weight-average molecular weight
NEM	<i>N</i> -Ethylmaleimide
NMM	<i>N</i> -Methylmorpholine
NMP	Nitroxide-mediated polymerization
NMR	Nuclear magnetic resonance
OEG	Oligo(ethylene glycol)
OEGA	Oligo(ethylene glycol) acrylate
OEGMA	Oligo(ethylene glycol)methacrylate
OPF	Oligo(poly(ethylene glycol) fumarate)
PAMs	Poly( <i>N</i> -alkylacrylamide)s
PAPi	Poly( <i>N</i> -acryloyl)pyrrolidine
PAPy	Poly( <i>N</i> -acryloyl)pyrrolidine
PBEEP	Poly(benzophenone ethylene ethyl phosphate)
PCL	Poly( $\epsilon$ -caprolactone)



PDEA	Poly( <i>N,N</i> -diethylacrylamide)
PDEGMA	Poly(diethylene glycol methyl ether methacrylate)
PDAs	Poly( <i>N,N</i> -dialkylacrylamide)s
PDEA	Poly( <i>N,N</i> -diethylacrylamide)
PDFEA	Poly[ <i>N</i> -(2,2-difluoroethyl)acrylamide]
PDLA	Polymer D-lactic acid
PDMAEMA	Poly(2-( <i>N,N</i> -dimethylamino) ethyl methacrylate)
PDMDOMA	Poly[ <i>N</i> -(2,2-dimethyl-1,3-dioxolane)-methyl] acrylamide
PDSEA	Pyridyldisulfide ethylacrylamide
PEG	Polyethylene glycol
PEGA	Poly(ethylene glycol acrylate)
PEGMA	Poly(ethylene glycol) methyl ether methacrylate
PEHO	Poly-(hydroxymethyl)oxetane
PEMA	Poly( <i>N,N</i> -ethylmethylacrylamide)
PEO	Poly(ethylene oxide)
PET	Photo-induced electron/energy transfer
PEtOx	Poly(2-ethyl-2-oxazoline)
PiPMA	Poly(isopropyl methacrylate)
PIPOx	Poly(2-isopropyl-2-oxazoline)
PI-RAFT	Photoiniferter reversible addition–fragmentation chain transfer
PLGA	Poly(lactic-co-glycolic acid)
PLLA	Poly(L-lactide)
PMEO <sub>2</sub> MA	Poly(2-(2-methoxyethoxy)ethyl methacrylate)
PMVE	Poly(methyl vinyl ether)
PNANPP	Poly( <i>N</i> -acryloyl- <i>N'</i> -propylpiperazine)
PNcPAM	Poly( <i>N</i> -cyclopropylacrylamide)
PNEAM	Poly( <i>N</i> -ethylacrylamide)
PNIPAM	Poly( <i>N</i> -isopropylacrylamide)
PNnPAM	Poly( <i>N</i> - <i>n</i> -propylacrylamide)
PNtBAM	Poly( <i>N</i> - <i>tert</i> -butylacrylamide)
PNVCL	Poly( <i>N</i> -vinylcaprolactam)
PNVIBA	Poly( <i>N</i> -vinylisobutyramide)
POEGMA	Poly(oligo(ethylene glycol)methacrylate)
POEGNB	Poly(oligoethylene glycol) norbornene
POEGSt	Poly(oligoethylene glycol) styrene
POEGVE	Poly(oligoethylene glycol) vinyl ether
poly(NMEP)	Poly( <i>N</i> -(2-methacryloyloxyethyl)pyrrolidone)
PPGMA	Poly(propylene glycol methacrylate)
PPO	Poly(propylene oxide)
PPrOx	Poly(2-propyl-2-oxazoline)
Pro	Proline
PSS	Polystyrene sulfonate
PVP/PVPy	Polyvinylpyrrolidone
RAFT	Reversible addition–fragmentation chain transfer
RGD	Arginine–glycine–aspartic acid
RGDS	Arginine–glycine–aspartic acid–serine
ROMP	Ring-opening metathesis polymerization
SARA	Supplemental activator and reducing agent
SANS	Small-angle neutron scattering
SAXS	Small-angle X-ray scattering
SEC	Size-exclusion chromatography
SEM	Scanning electron microscopy
Sn(EH) <sub>2</sub>	Tin(II) 2-ethylhexanoate
<i>T</i> <sub>cp</sub>	Cloud point temperature

TEM	Transmission electron microscopy
TGA	Thermogravimetric analysis
TPMA	Tris(2-pyridylmethyl)amine
TREN	Tris(2-aminoethyl)amine
XPS	X-ray photoelectron spectroscopy
XRD	X-ray powder diffraction

## Conflicts of interest

There are no conflicts to declare.

## Acknowledgements

This study was financially supported by Case Western Reserve University (CWRU) College of Arts and Science (CAS) and Expanding Horizons Initiative at CWRU. YY thanks CWRU Flora Stone Mather Center for Women for financial support.

## References

- S. Dai, P. Ravi and K. C. Tam, *Soft Matter*, 2009, **5**, 2513–2533.
- Y.-J. Kim and Y. T. Matsunaga, *J. Mater. Chem. B*, 2017, **5**, 4307–4321.
- M. T. Cook, P. Haddow, S. B. Kirton and W. J. McAuley, *Adv. Funct. Mater.*, 2021, **31**, 2008123.
- F. Doberenz, K. Zeng, C. Willems, K. Zhang and T. Groth, *J. Mater. Chem. B*, 2020, **8**, 607–628.
- P. Zarrintaj, M. Jouyandeh, M. R. Ganjali, B. S. Hadavand, M. Mozafari, S. S. Sheiko, M. Vatankhah-Varnoosfaderani, T. J. Gutiérrez and M. R. Saeb, *Eur. Polym. J.*, 2019, **117**, 402–423.
- O. Bertrand and J.-F. Gohy, *Polym. Chem.*, 2017, **8**, 52–73.
- Y. Takashima, S. Hatanaka, M. Otsubo, M. Nakahata, T. Kakuta, A. Hashidzume, H. Yamaguchi and A. Harada, *Nat. Commun.*, 2012, **3**, 1270.
- F. D. Jochum, L. zur Borg, P. J. Roth and P. Theato, *Macromolecules*, 2009, **42**, 7854–7862.
- J. Jiang, X. Tong and Y. Zhao, *J. Am. Chem. Soc.*, 2005, **127**, 8290–8291.
- G. Kocak, C. Tuncer and V. Bütün, *Polym. Chem.*, 2017, **8**, 144–176.
- S. Dai, P. Ravi and K. C. Tam, *Soft Matter*, 2008, **4**, 435–449.
- A. Nese, N. V. Lebedeva, G. Sherwood, S. Averick, Y. Li, H. Gao, L. Peteanu, S. S. Sheiko and K. Matyjaszewski, *Macromolecules*, 2011, **44**, 5905–5910.
- M. Kohri, K. Yanagimoto, K. Kohaku, S. Shiimoto, M. Kobayashi, A. Imai, F. Shiba, T. Taniguchi and K. Kishikawa, *Macromolecules*, 2018, **51**, 6740–6745.
- K. Ulbrich, K. Holá, V. Šubr, A. Bakandritsos, J. Tuček and R. Zbořil, *Chem. Rev.*, 2016, **116**, 5338–5431.
- M. Czaun, L. Hevesi, M. Takafuji and H. Ihara, *Chem. Commun.*, 2008, 2124–2126, DOI: [10.1039/b717721f](https://doi.org/10.1039/b717721f).





- 16 P. M. Xulu, G. Filipcsei and M. Zrínyi, *Macromolecules*, 2000, **33**, 1716–1719.
- 17 T. Tanaka, I. Nishio, S.-T. Sun and S. Ueno-Nishio, *Science*, 1982, **218**, 467–469.
- 18 T. Shiga, *Neutron Spin Echo Spectroscopy Viscoelasticity Rheology*, Springer Berlin Heidelberg, Berlin, Heidelberg, 1997, pp. 131–163. DOI: [10.1007/3-540-68449-2\\_2](https://doi.org/10.1007/3-540-68449-2_2).
- 19 S. Ramanathan and L. H. Block, *J. Controlled Release*, 2001, **70**, 109–123.
- 20 J. Kost, K. Leong and R. Langer, *Proc. Natl. Acad. Sci. U. S. A.*, 1989, **86**, 7663–7666.
- 21 A. Marin, M. Muniruzzaman and N. Rapoport, *J. Controlled Release*, 2001, **75**, 69–81.
- 22 J. Li, C. Nagamani and J. S. Moore, *Acc. Chem. Res.*, 2015, **48**, 2181–2190.
- 23 Y. C. Simon and S. L. Craig, *Mechanochemistry in Materials*, Royal Society of Chemistry, 2017.
- 24 M. A. C. Stuart, W. T. S. Huck, J. Genzer, M. Muller, C. Ober, M. Stamm, G. B. Sukhorukov, I. Szleifer, V. V. Tsukruk, M. Urban, F. Winnik, S. Zauscher, I. Luzinov and S. Minko, *Nat. Mater.*, 2010, **9**, 101–113.
- 25 D. Roy, J. N. Cambre and B. S. Sumerlin, *Prog. Polym. Sci.*, 2010, **35**, 278–301.
- 26 D. Roy, W. L. A. Brooks and B. S. Sumerlin, *Chem. Soc. Rev.*, 2013, **42**, 7214–7243.
- 27 M. Wei, Y. Gao, X. Li and M. J. Serpe, *Polym. Chem.*, 2017, **8**, 127–143.
- 28 A. P. Vogt and B. S. Sumerlin, *Soft Matter*, 2009, **5**, 2347–2351.
- 29 J. S. Scarpa, D. D. Mueller and I. M. Klotz, *J. Am. Chem. Soc.*, 1967, **89**, 6024–6030.
- 30 M. Heskins and J. E. Guillet, *J. Macromol. Sci., Chem.*, 1968, **2**, 1441–1455.
- 31 S. Fujishige, K. Kubota and I. Ando, *J. Phys. Chem.*, 1989, **93**, 3311–3313.
- 32 M. Lemanowicz, A. Gierczycki, W. Kuźnik, R. Sancewicz and P. Imiela, *Miner. Eng.*, 2014, **69**, 170–176.
- 33 J. C. Foster, I. Akar, M. C. Grocott, A. K. Pearce, R. T. Mathers and R. K. O'Reilly, *ACS Macro Lett.*, 2020, **9**, 1700–1707.
- 34 A. Narumi, S.-i. Sato, X. Shen and T. Kakuchi, *Polym. Chem.*, 2022, **13**, 1293–1319.
- 35 A. Bordat, T. Boissenot, J. Nicolas and N. Tsapis, *Adv. Drug Delivery Rev.*, 2019, **138**, 167–192.
- 36 M. Shibayama and T. Tanaka, in *Responsive Gels: Volume Transitions I*, ed. K. Dušek, Springer Berlin Heidelberg, Berlin, Heidelberg, 1993, pp. 1–62. DOI: [10.1007/3-540-56791-7\\_1](https://doi.org/10.1007/3-540-56791-7_1).
- 37 G. Chen and A. S. Hoffman, *Nature*, 1995, **373**, 49–52.
- 38 H. Feil, Y. H. Bae, J. Feijen and S. W. Kim, *Macromolecules*, 1993, **26**, 2496–2500.
- 39 X. Qiu, T. Koga, F. Tanaka and F. M. Winnik, *Sci. China: Chem.*, 2013, **56**, 56–64.
- 40 G. Pasparakis and C. Tsitsilianis, *Polymer*, 2020, **211**, 123146.
- 41 H. G. Schild, *Prog. Polym. Sci.*, 1992, **17**, 163–249.
- 42 R. Liu, M. Fraylich and B. R. Saunders, *Colloid Polym. Sci.*, 2009, **287**, 627–643.
- 43 Z. Hu, T. Cai and C. Chi, *Soft Matter*, 2010, **6**, 2115–2123.
- 44 V. Aseyev, H. Tenhu and F. M. Winnik, in *Self Organized Nanostructures of Amphiphilic Block Copolymers II*, ed. A. H. E. Müller and O. Borisov, Springer Berlin Heidelberg, Berlin, Heidelberg, 2011, pp. 29–89. DOI: [10.1007/12\\_2010\\_57](https://doi.org/10.1007/12_2010_57).
- 45 G. Vancoillie, D. Frank and R. Hoogenboom, *Prog. Polym. Sci.*, 2014, **39**, 1074–1095.
- 46 A. Halperin, M. Kröger and F. M. Winnik, *Angew. Chem., Int. Ed.*, 2015, **54**, 15342–15367.
- 47 Q. Zhang, C. Weber, U. S. Schubert and R. Hoogenboom, *Mater. Horiz.*, 2017, **4**, 109–116.
- 48 R. Hoogenboom, in *Smart Polymers and their Applications*, ed. M. R. Aguilar and J. San Román, Woodhead Publishing, 2nd edn, 2019, pp. 13–44. DOI: [10.1016/B978-0-08-102416-4.00002-8](https://doi.org/10.1016/B978-0-08-102416-4.00002-8).
- 49 C. Zhao, Z. Ma and X. X. Zhu, *Prog. Polym. Sci.*, 2019, **90**, 269–291.
- 50 X. Chen, J. Zhang, K. Wu, X. Wu, J. Tang, S. Cui, D. Cao, R. Liu, C. Peng, L. Yu and J. Ding, *Small Methods*, 2020, **4**, 2000310.
- 51 P. Gheysoori, A. Paydayesh, M. Jafari and H. Peidayesh, *Eur. Polym. J.*, 2023, **186**, 111846.
- 52 D. Iohara, M. Okubo, M. Anraku, S. Uramatsu, T. Shimamoto, K. Uekama and F. Hirayama, *Mol. Pharmaceutics*, 2017, **14**, 2740–2748.
- 53 S. Kim, K. Lee and C. Cha, *J. Biomater. Sci., Polym. Ed.*, 2016, **27**, 1698–1711.
- 54 J. Li, J. Leng, Y. Qu, L. Deng and J. Ren, *Mater. Lett.*, 2014, **131**, 5–8.
- 55 A. K. Bajpai, S. K. Shukla, S. Bhanu and S. Kankane, *Prog. Polym. Sci.*, 2008, **33**, 1088–1118.
- 56 G.-H. Hsiue, R.-W. Chang, C.-H. Wang and S.-H. Lee, *Biomaterials*, 2003, **24**, 2423–2430.
- 57 A. Alexander, Ajazuddin, J. Khan, S. Saraf and S. Saraf, *Eur. J. Pharm. Biopharm.*, 2014, **88**, 575–585.
- 58 A. Alexander, Ajazuddin, J. Khan, S. Saraf and S. Saraf, *J. Controlled Release*, 2013, **172**, 715–729.
- 59 M. Patenaude and T. Hoare, *ACS Macro Lett.*, 2012, **1**, 409–413.
- 60 Z. W. Cui, B. H. Lee, C. Pauken and B. L. Vernon, *J. Biomed. Mater. Res., Part A*, 2011, **98A**, 159–166.
- 61 W. X. Wang, H. Liang, R. C. Al Ghanami, L. Hamilton, M. Fraylich, K. M. Shakesheff, B. Saunders and C. Alexander, *Adv. Mater.*, 2009, **21**, 1809–1813.
- 62 E. Henderson, B. H. Lee, Z. W. Cui, R. McLemore, T. A. Brandon and B. L. Vernon, *J. Biomed. Mater. Res., Part A*, 2009, **90A**, 1186–1197.
- 63 S. Fu, G. Guo, C. Gong, S. Zeng, H. Liang, F. Luo, X. Zhang, X. Zhao, Y. Wei and Z. Qian, *J. Phys. Chem. B*, 2009, **113**, 16518–16525.
- 64 M. Sponchioni, N. Manfredini, A. Zanoni, E. Scibona, M. Morbidelli and D. Moscatelli, *ACS Biomater. Sci. Eng.*, 2020, **6**, 5337–5345.



- 65 K. Nagase, M. Yamato, H. Kanazawa and T. Okano, *Biomaterials*, 2018, **153**, 27–48.
- 66 T. Koriyama, Y. Takayama, C. Hisatsune, T. A. Asoh and A. Kikuchi, *J. Biomater. Sci., Polym. Ed.*, 2017, **28**, 900–912.
- 67 J. Kobayashi, M. Yamato and T. Okano, *J. Biomater. Sci., Polym. Ed.*, 2017, **28**, 939–957.
- 68 H. Takahashi, M. Nakayama, K. Itoga, M. Yamato and T. Okano, *Biomacromolecules*, 2011, **12**, 1414–1418.
- 69 Q. Yu, Y. Zhang, H. Chen, F. Zhou, Z. Wu, H. Huang and J. L. Brash, *Langmuir*, 2010, **26**, 8582–8588.
- 70 K. Uhlig, E. Wischerhoff, J. F. Lutz, A. Laschewsky, M. S. Jaeger, A. Lankenau and C. Duschl, *Soft Matter*, 2010, **6**, 4262–4267.
- 71 T. Chen, R. Ferris, J. Zhang, R. Ducker and S. Zauscher, *Prog. Polym. Sci.*, 2010, **35**, 94–112.
- 72 A. Mizutani, A. Kikuchi, M. Yamato, H. Kanazawa and T. Okano, *Biomaterials*, 2008, **29**, 2073–2081.
- 73 P. M. Mendes, *Chem. Soc. Rev.*, 2008, **37**, 2512–2529.
- 74 H. Hatakeyama, A. Kikuchi, M. Yamato and T. Okano, *Biomaterials*, 2007, **28**, 3632–3643.
- 75 N. Nath and A. Chilkoti, *Adv. Mater.*, 2002, **14**, 1243–1247.
- 76 S. Forg, A. Karbacher, Z. Ye, X. Guo and R. von Klitzing, *Langmuir*, 2022, **38**, 5275–5285.
- 77 K. J. Hogan and A. G. Mikos, *Polymer*, 2020, **211**, 123063.
- 78 M. Sponchioni, U. Capasso Palmiero and D. Moscatelli, *Mater. Sci. Eng., C*, 2019, **102**, 589–605.
- 79 M. H. Bhuiyan, A. N. Clarkson and M. A. Ali, *Colloids Surf., B*, 2023, **224**, 113193.
- 80 S. Ashraf, H.-K. Park, H. Park and S.-H. Lee, *Macromol. Res.*, 2016, **24**, 297–304.
- 81 H. Vihola, A. Laukkanen, L. Valtola, H. Tenhu and J. Hirvonen, *Biomaterials*, 2005, **26**, 3055–3064.
- 82 X. Wang, X. Qiu and C. Wu, *Macromolecules*, 1998, **31**, 2972–2976.
- 83 F. Tanimoto, Y. Kitamura, T. Ono and H. Yoshizawa, *ACS Appl. Mater. Interfaces*, 2010, **2**, 606–610.
- 84 S. Tang, M. Floy, R. Bhandari, M. Sunkara, A. J. Morris, T. D. Dziubla and J. Z. Hilt, *ACS Omega*, 2017, **2**, 8723–8729.
- 85 J.-F. Lutz, Ö. Akdemir and A. Hoth, *J. Am. Chem. Soc.*, 2006, **128**, 13046–13047.
- 86 B. Yıldız, B. Işık and M. Kış, *Polymer*, 2001, **42**, 2521–2529.
- 87 G. Fundueanu, M. Constantin, F. Bortolotti, P. Ascenzi, R. Cortesi and E. Menegatti, *Macromol. Biosci.*, 2005, **5**, 955–964.
- 88 Y. Huang, P. Yong, Y. Chen, Y. Gao, W. Xu, Y. Lv, L. Yang, R. L. Reis, R. P. Pirracco and J. Chen, *RSC Adv.*, 2017, **7**, 28711–28722.
- 89 S. Senel, B. Isik-Yuruksoy, H. Cicek and A. Tuncel, *J. Appl. Polym. Sci.*, 1997, **64**, 1775–1784.
- 90 K. Nagase, A. Ota, T. Hirotani, S. Yamada, A. M. Akimoto and H. Kanazawa, *Macromol. Rapid Commun.*, 2020, **41**, 2000308.
- 91 Y. Nakayama, R. Okahashi, R. Iwai and K. Uchida, *Langmuir*, 2007, **23**, 8206–8211.
- 92 Y. Maeda, T. Nakamura and I. Ikeda, *Macromolecules*, 2001, **34**, 1391–1399.
- 93 D. Ito and K. Kubota, *Macromolecules*, 1997, **30**, 7828–7834.
- 94 J. Xu, X. Jiang and S. Liu, *J. Polym. Sci., Part A: Polym. Chem.*, 2008, **46**, 60–69.
- 95 I. Idziak, D. Avoce, D. Lessard, D. Gravel and X. X. Zhu, *Macromolecules*, 1999, **32**, 1260–1263.
- 96 M. Mertoglu, S. Garnier, A. Laschewsky, K. Skrabania and J. Storsberg, *Polymer*, 2005, **46**, 7726–7740.
- 97 X. Huang, F. Du, R. Ju and Z. Li, *Macromol. Rapid Commun.*, 2007, **28**, 597–603.
- 98 Y. Akiyama, Y. Shinohara, Y. Hasegawa, A. Kikuchi and T. Okano, *J. Polym. Sci., Part A: Polym. Chem.*, 2008, **46**, 5471–5482.
- 99 Y. Zou, D. E. Brooks and J. N. Kizhakkedathu, *Macromolecules*, 2008, **41**, 5393–5405.
- 100 N. Badi, *Prog. Polym. Sci.*, 2017, **66**, 54–79.
- 101 X. Tao, K. Liu, W. Li and A. Zhang, *Polymer*, 2014, **55**, 3672–3679.
- 102 L. Liu, W. Li, K. Liu, J. Yan, G. Hu and A. Zhang, *Macromolecules*, 2011, **44**, 8614–8621.
- 103 J. F. Lutz, *Adv. Mater.*, 2011, **23**, 2237–2243.
- 104 S. Han, M. Hagiwara and T. Ishizone, *Macromolecules*, 2003, **36**, 8312–8319.
- 105 T. Ishizone, A. Seki, M. Hagiwara, S. Han, H. Yokoyama, A. Oyane, A. Deffieux and S. Carlotti, *Macromolecules*, 2008, **41**, 2963–2967.
- 106 J.-F. Lutz, K. Weichenhan, Ö. Akdemir and A. Hoth, *Macromolecules*, 2007, **40**, 2503–2508.
- 107 T. Cai, M. Marquez and Z. Hu, *Langmuir*, 2007, **23**, 8663–8666.
- 108 C. Boyer, M. R. Whittaker, M. Luzon and T. P. Davis, *Macromolecules*, 2009, **42**, 6917–6926.
- 109 Y. Guo, X. Dong, W. Ruan, Y. Shang and H. Liu, *Colloid Polym. Sci.*, 2017, **295**, 327–340.
- 110 J. F. Lutz and A. Hoth, *Macromolecules*, 2006, **39**, 893–896.
- 111 B. Zhao, D. Li, F. Hua and D. R. Green, *Macromolecules*, 2005, **38**, 9509–9517.
- 112 S. Aoshima, H. Oda and E. Kobayashi, *J. Polym. Sci., Part A: Polym. Chem.*, 1992, **30**, 2407–2413.
- 113 T. Bauer and C. Slugovc, *J. Polym. Sci., Part A: Polym. Chem.*, 2010, **48**, 2098–2108.
- 114 T. Isono, K. Miyachi, Y. Satoh, S.-i. Sato, T. Kakuchi and T. Satoh, *Polym. Chem.*, 2017, **8**, 5698–5707.
- 115 T. He, Y. Wang, L. Xu, X. Fu, A. Narumi, S.-i. Sato, X. Shen and T. Kakuchi, *Polym. Chem.*, 2021, **12**, 2580–2591.
- 116 X. Jiang, M. R. Smith and G. L. Baker, *Macromolecules*, 2008, **41**, 318–324.
- 117 X. Jiang, E. B. Vogel, M. R. Smith and G. L. Baker, *Macromolecules*, 2008, **41**, 1937–1944.
- 118 H. Shimomoto, K. Shimizu, C. Takeda, M. Kikuchi, T. Kudo, H. Mukai, T. Itoh, E. Ihara, N. Hoshikawa, A. Koiwai and N. Hasegawa, *Polym. Chem.*, 2015, **6**, 8124–8131.
- 119 H. R. Allcock and G. K. Dudley, *Macromolecules*, 1996, **29**, 1313–1319.



- 120 H. R. Allcock, S. R. Pucher, M. L. Turner and R. J. Fitzpatrick, *Macromolecules*, 1992, **25**, 5573–5577.
- 121 C. Geng, S. Wang and H. Wang, *Polymers*, 2021, **13**, 1813.
- 122 X. Fu, Y. Shen, W. Fu and Z. Li, *Macromolecules*, 2013, **46**, 3753–3760.
- 123 Y. Haba, A. Harada, T. Takagishi and K. Kono, *J. Am. Chem. Soc.*, 2004, **126**, 12760–12761.
- 124 C. de las Heras Alarcón, S. Pennadam and C. Alexander, *Chem. Soc. Rev.*, 2005, **34**, 276–285.
- 125 S. Hocine and M.-H. Li, *Soft Matter*, 2013, **9**, 5839–5861.
- 126 A. Crespo Colin, S. M. Cancho, R. G. Rubio and A. Compostizo, *Phys. Chem. Chem. Phys.*, 1999, **1**, 319–322.
- 127 P. Alexandridis and T. Alan Hatton, *Colloids Surf., A*, 1995, **96**, 1–46.
- 128 P. Alexandridis, J. F. Holzwarth and T. A. Hatton, *Macromolecules*, 1994, **27**, 2414–2425.
- 129 K. Suwa, Y. Wada, Y. Kikunaga, K. Morishita, A. Kishida and M. Akashi, *J. Polym. Sci., Part A: Polym. Chem.*, 1997, **35**, 1763–1768.
- 130 L. H. Gan, Y. Y. Gan and G. R. Deen, *Macromolecules*, 2000, **33**, 7893–7897.
- 131 Y. Maeda, T. Nakamura and I. Ikeda, *Macromolecules*, 2002, **35**, 217–222.
- 132 N. Vanparijs, L. Nuhn and B. G. De Geest, *Chem. Soc. Rev.*, 2017, **46**, 1193–1239.
- 133 W. Z. Zhang, X. D. Chen, W. Luo, J. Yang, M. Q. Zhang and F. M. Zhu, *Macromolecules*, 2009, **42**, 1720–1725.
- 134 H. Mori, H. Iwaya, A. Nagai and T. Endo, *Chem. Commun.*, 2005, 4872–4874, DOI: [10.1039/b509212d](https://doi.org/10.1039/b509212d).
- 135 Z. L. Liu, J. W. Hu, J. P. Sun, G. P. He, Y. H. Li and G. W. Zhang, *J. Polym. Sci., Part A: Polym. Chem.*, 2010, **48**, 3573–3586.
- 136 N. A. Cortez-Lemus and A. Licea-Claverie, *Prog. Polym. Sci.*, 2016, **53**, 1–51.
- 137 A. C. W. Lau and C. Wu, *Macromolecules*, 1999, **32**, 581–584.
- 138 L. Marsili, M. Dal Bo, G. Eisele, I. Donati, F. Berti and G. Toffoli, *Polymers*, 2021, **13**, 2639.
- 139 C. Weber, C. R. Becer, R. Hoogenboom and U. S. Schubert, *Macromolecules*, 2009, **42**, 2965–2971.
- 140 C. Weber, R. Hoogenboom and U. S. Schubert, *Prog. Polym. Sci.*, 2012, **37**, 686–714.
- 141 R. Hoogenboom and H. Schlaad, *Polym. Chem.*, 2017, **8**, 24–40.
- 142 U. Hiroshi and K. Shiro, *Chem. Lett.*, 1992, **21**, 1643–1646.
- 143 M. M. Bloksma, R. M. Paulus, H. P. C. van Kuringen, F. van der Woerd, H. M. L. Lambermont-Thijs, U. S. Schubert and R. Hoogenboom, *Macromol. Rapid Commun.*, 2012, **33**, 92–96.
- 144 X. Song, Y. Wen, J.-L. Zhu, F. Zhao, Z.-X. Zhang and J. Li, *Biomacromolecules*, 2016, **17**, 3957–3963.
- 145 H. Liu, J. Zhang, X. Luo, N. Kong, L. Cui and J. Liu, *Eur. Polym. J.*, 2013, **49**, 2949–2960.
- 146 P. S. Stayton, T. Shimoboji, C. Long, A. Chilkoti, G. Ghen, J. M. Harris and A. S. Hoffman, *Nature*, 1995, **378**, 472–474.
- 147 C. Li, C. Wang, Z. Ji, N. Jiang, W. Lin and D. Li, *Eur. Polym. J.*, 2019, **113**, 404–410.
- 148 X. Savelyeva and M. Marić, *J. Polym. Sci., Part A: Polym. Chem.*, 2014, **52**, 2011–2024.
- 149 O. W. Webster, W. R. Hertler, D. Y. Sogah, W. B. Farnham and T. V. RajanBabu, *J. Am. Chem. Soc.*, 1983, **105**, 5706–5708.
- 150 K. Fuchise, Y. Chen, T. Satoh and T. Kakuchi, *Polym. Chem.*, 2013, **4**, 4278–4291.
- 151 P. Zhang, P. She, J. He, Z. Xiang, Z. Li, Y. Cao and X. Zhang, *React. Funct. Polym.*, 2019, **142**, 128–133.
- 152 M. Teodorescu and K. Matyjaszewski, *Macromolecules*, 1999, **32**, 4826–4831.
- 153 K. Matyjaszewski and J. Xia, *Chem. Rev.*, 2001, **101**, 2921–2990.
- 154 W. A. Braunecker and K. Matyjaszewski, *Prog. Polym. Sci.*, 2007, **32**, 93–146.
- 155 K. Matyjaszewski, *Macromolecules*, 2012, **45**, 4015–4039.
- 156 G. Moad, E. Rizzardo and S. H. Thang, *Aust. J. Chem.*, 2005, **58**, 379–410.
- 157 G. Moad, *Polym. Chem.*, 2017, **8**, 177–219.
- 158 A. E. Smith, X. Xu and C. L. McCormick, *Prog. Polym. Sci.*, 2010, **35**, 45–93.
- 159 W. Wang, H. Liang, R. Cheikh Al Ghanami, L. Hamilton, M. Fraylich, K. M. Shakesheff, B. Saunders and C. Alexander, *Adv. Mater.*, 2009, **21**, 1809–1813.
- 160 G. Masci, L. Giacomelli and V. Crescenzi, *Macromol. Rapid Commun.*, 2004, **25**, 559–564.
- 161 P. Chmielarz, P. Kryszewski, S. Park and K. Matyjaszewski, *Polymer*, 2015, **71**, 143–147.
- 162 W. Jakubowski and K. Matyjaszewski, *Angew. Chem., Int. Ed.*, 2006, **45**, 4482–4486.
- 163 J. R. Adams and S. K. Mallapragada, *Macromol. Chem. Phys.*, 2013, **214**, 1321–1325.
- 164 T. G. Ribelli, M. Fantin, J.-C. Daran, K. F. Augustine, R. Poli and K. Matyjaszewski, *J. Am. Chem. Soc.*, 2018, **140**, 1525–1534.
- 165 S. d. Á. Gonçalves and R. P. Vieira, *React. Funct. Polym.*, 2020, **147**, 104453.
- 166 Y.-Y. Liu, Y.-B. Zhong, J.-K. Nan and W. Tian, *Macromolecules*, 2010, **43**, 10221–10230.
- 167 Z. Gao, J. Liang, X. Tao, Y. Cui, T. Satoh, T. Kakuchi and Q. Duan, *Macromol. Res.*, 2012, **20**, 508–514.
- 168 Z.-X. Zhang, X. Liu, F. J. Xu, X. J. Loh, E.-T. Kang, K.-G. Neoh and J. Li, *Macromolecules*, 2008, **41**, 5967–5970.
- 169 P. Pan, M. Fujita, W.-Y. Ooi, K. Sudesh, T. Takarada, A. Goto and M. Maeda, *Langmuir*, 2012, **28**, 14347–14356.
- 170 M. Karayilan, K. C. McCleary-Petersen, M. O. B. Hamilton, L. Fu, K. Matyjaszewski, R. S. Glass, D. L. Lichtenberger and J. Pyun, *Macromol. Rapid Commun.*, 2020, **41**, 1900424.
- 171 C.-W. Chang, E. Bays, L. Tao, S. N. S. Alconcel and H. D. Maynard, *Chem. Commun.*, 2009, 3580–3582, DOI: [10.1039/B904456F](https://doi.org/10.1039/B904456F).
- 172 D. Pissuwan, C. Boyer, K. Gunasekaran, T. P. Davis and V. Bulmus, *Biomacromolecules*, 2010, **11**, 412–420.



- 173 B. D. Fairbanks, P. A. Gunatillake and L. Meagher, *Adv. Drug Delivery Rev.*, 2015, **91**, 141–152.
- 174 J. M. Spruell, B. A. Levy, A. Sutherland, W. R. Dichtel, J. Y. Cheng, J. F. Stoddart and A. Nelson, *J. Polym. Sci., Part A: Polym. Chem.*, 2009, **47**, 346–356.
- 175 H. Willcock and R. K. O'Reilly, *Polym. Chem.*, 2010, **1**, 149–157.
- 176 F. Ganachaud, M. J. Monteiro, R. G. Gilbert, M.-A. Dourges, S. H. Thang and E. Rizzardo, *Macromolecules*, 2000, **33**, 6738–6745.
- 177 C. Schilli, M. G. Lanzendörfer and A. H. E. Müller, *Macromolecules*, 2002, **35**, 6819–6827.
- 178 A. J. Convertine, N. Ayres, C. W. Scales, A. B. Lowe and C. L. McCormick, *Biomacromolecules*, 2004, **5**, 1177–1180.
- 179 A. J. Convertine, B. S. Lokitz, Y. Vasileva, L. J. Myrick, C. W. Scales, A. B. Lowe and C. L. McCormick, *Macromolecules*, 2006, **39**, 1724–1730.
- 180 S. Perrier, *Macromolecules*, 2017, **50**, 7433–7447.
- 181 M. Morimura, S. Ida, M. Oyama, H. Takeshita and S. Kanaoka, *Macromolecules*, 2021, **54**, 1732–1741.
- 182 R. Plummer, D. J. T. Hill and A. K. Whittaker, *Macromolecules*, 2006, **39**, 8379–8388.
- 183 J. Xu, S. Luo, W. Shi and S. Liu, *Langmuir*, 2006, **22**, 989–997.
- 184 C. Herfurth, A. Laschewsky, L. Noirez, B. von Lospichl and M. Gradziński, *Polymer*, 2016, **107**, 422–433.
- 185 M. Cao, H. Nie, Y. Hou, G. Han and W. Zhang, *Polym. Chem.*, 2019, **10**, 403–411.
- 186 M. L. Allegranza and D. Konkolewicz, *ACS Macro Lett.*, 2021, **10**, 433–446.
- 187 S. Xu, F. J. Trujillo, J. Xu, C. Boyer and N. Corrigan, *Macromol. Rapid Commun.*, 2021, **42**, 2100212.
- 188 A. Sivokhin, D. Orekhov, O. Kazantsev, O. Sivokhina, S. Orekhov, D. Kamorin, K. Otopkova, M. Smirnov and R. Karpov, *Polymers*, 2022, **14**, 137.
- 189 K. Nagase, T. Onuma, M. Yamato, N. Takeda and T. Okano, *Macromol. Rapid Commun.*, 2015, **36**, 1965–1970.
- 190 F. Liu, C.-H. Du, B.-K. Zhu and Y.-Y. Xu, *Polymer*, 2007, **48**, 2910–2918.
- 191 Z. Zhang, A. J. Morse, S. P. Armes, A. L. Lewis, M. Geoghegan and G. J. Leggett, *Langmuir*, 2011, **27**, 2514–2521.
- 192 A. Olivier, F. Meyer, J.-M. Raquez, P. Damman and P. Dubois, *Prog. Polym. Sci.*, 2012, **37**, 157–181.
- 193 G. Conzatti, S. Cavalie, C. Combes, J. Torrisani, N. Carrere and A. Tournette, *Colloids Surf., B*, 2017, **151**, 143–155.
- 194 B. Zdyrko and I. Luzinov, *Macromol. Rapid Commun.*, 2011, **32**, 859–869.
- 195 L. Wu, U. Glebe and A. Böker, *Polym. Chem.*, 2015, **6**, 5143–5184.
- 196 R. Barbey, L. Lavanant, D. Paripovic, N. Schüwer, C. Sugnaux, S. Tugulu and H.-A. Klok, *Chem. Rev.*, 2009, **109**, 5437–5527.
- 197 P. Shivapooja, L. K. Ista, H. E. Canavan and G. P. Lopez, *Biointerphases*, 2012, **7**, 32.
- 198 B. Lego, M. François, W. G. Skene and S. Giasson, *Langmuir*, 2009, **25**, 5313–5321.
- 199 S. Edmondson, V. L. Osborne and W. T. S. Huck, *Chem. Soc. Rev.*, 2004, **33**, 14–22.
- 200 M. Krishnamoorthy, S. Hakobyan, M. Ramstedt and J. E. Gautrot, *Chem. Rev.*, 2014, **114**, 10976–11026.
- 201 L. W. Teunissen, A. R. Kuzmyn, F. S. Ruggeri, M. M. J. Smulders and H. Zuillhof, *Adv. Mater. Interfaces*, 2022, **9**, 2101717.
- 202 P.-F. Guo, H.-Y. Gong, H.-W. Zheng, M.-L. Chen, J.-H. Wang and L. Ye, *Colloids Surf., B*, 2020, **196**, 111282.
- 203 A. Khabibullin, E. Mastan, K. Matyjaszewski and S. Zhu, in *Controlled Radical Polymerization at and from Solid Surfaces*, ed. P. Vana, Springer International Publishing, Cham, 2016, pp. 29–76. DOI: [10.1007/12\\_2015\\_311](https://doi.org/10.1007/12_2015_311).
- 204 N. Matsuzaka, H. Takahashi, M. Nakayama, A. Kikuchi and T. Okano, *J. Biomater. Sci., Polym. Ed.*, 2012, **23**, 1301–1314.
- 205 A. B. Lowe and C. L. McCormick, *Prog. Polym. Sci.*, 2007, **32**, 283–351.
- 206 R. D. Roeder, O. Garcia-Valdez, R. A. Whitney, P. Champagne and M. F. Cunningham, *Polym. Chem.*, 2016, **7**, 6383–6390.
- 207 M. Li, M. Fromel, D. Ranaweera, S. Rocha, C. Boyer and C. W. Pester, *ACS Macro Lett.*, 2019, **8**, 374–380.
- 208 A. R. Kuzmyn, A. T. Nguyen, L. W. Teunissen, H. Zuillhof and J. Baggerman, *Langmuir*, 2020, **36**, 4439–4446.
- 209 A. R. Kuzmyn, L. W. Teunissen, P. Fritz, B. van Lagen, M. M. J. Smulders and H. Zuillhof, *Adv. Mater. Interfaces*, 2022, **9**, 2101784.
- 210 J. E. Krause, N. D. Brault, Y. Li, H. Xue, Y. Zhou and S. Jiang, *Macromolecules*, 2011, **44**, 9213–9220.
- 211 H. Cheng, S. Xie, Y. Zhou, W. Huang, D. Yan, J. Yang and B. Ji, *J. Phys. Chem. B*, 2010, **114**, 6291–6299.
- 212 W. Steinhauer, R. Hoogenboom, H. Keul and M. Moeller, *Macromolecules*, 2013, **46**, 1447–1460.
- 213 W. Sun, Z. An and P. Wu, *Macromol. Rapid Commun.*, 2017, **38**, 1600808.
- 214 N. Fechner, N. Badi, K. Schade, S. Pfeifer and J.-F. Lutz, *Macromolecules*, 2009, **42**, 33–36.
- 215 N. Badi and J.-F. Lutz, *J. Controlled Release*, 2009, **140**, 224–229.
- 216 W. Li, A. Zhang, Y. Chen, K. Feldman, H. Wu and A. D. Schlüter, *Chem. Commun.*, 2008, 5948–5950, DOI: [10.1039/B814192D](https://doi.org/10.1039/B814192D).
- 217 L. Feng, Y. Liu, J. Hao, X. Li, C. Xiong and X. Deng, *Macromol. Chem. Phys.*, 2011, **212**, 2626–2632.
- 218 G.-F. Luo, W.-H. Chen and X.-Z. Zhang, *ACS Macro Lett.*, 2020, **9**, 872–881.
- 219 J. E. Chung, M. Yokoyama, M. Yamato, T. Aoyagi, Y. Sakurai and T. Okano, *J. Controlled Release*, 1999, **62**, 115–127.
- 220 M. Arotçaréna, B. Heise, S. Ishaya and A. Laschewsky, *J. Am. Chem. Soc.*, 2002, **124**, 3787–3793.
- 221 J. A. Jaber and J. B. Schlenoff, *Macromolecules*, 2005, **38**, 1300–1306.





- 222 G. Fundueanu, M. Constantin, S. Bucatariu and P. Ascenzi, *eXPRESS Polym. Lett.*, 2020, **14**, 63–76.
- 223 M. L. Ohnsorg, J. M. Ting, S. D. Jones, S. Jung, F. S. Bates and T. M. Reineke, *Polym. Chem.*, 2019, **10**, 3469–3479.
- 224 X. Lang, A. D. Patrick, B. Hammouda and M. J. A. Hore, *Polymer*, 2018, **145**, 137–147.
- 225 Y. Xia, N. A. D. Burke and H. D. H. Stöver, *Macromolecules*, 2006, **39**, 2275–2283.
- 226 N. Xue, X.-P. Qiu, Y. Chen, T. Satoh, T. Kakuchi and F. M. Winnik, *J. Polym. Sci., Part B: Polym. Phys.*, 2016, **54**, 2059–2068.
- 227 K. Zhu, R. Pamies, N. Al-Manasir, J. Ginés Hernández Cifre, J. García de la Torre, B. Nyström and A.-L. Kjøniksen, *ChemPhysChem*, 2020, **21**, 1258–1271.
- 228 Y. Chen, N. Xiao, M. Fukuoka, K. Yoshida, Q. Duan, T. Satoh and T. Kakuchi, *Polym. Chem.*, 2015, **6**, 3608–3616.
- 229 H. H. Nguyen, B. Payré, J. Fitremann, N. Lauth-de Viguerie and J.-D. Marty, *Langmuir*, 2015, **31**, 4761–4768.
- 230 X.-P. Qiu, F. Tanaka and F. M. Winnik, *Macromolecules*, 2007, **40**, 7069–7071.
- 231 J. Xu, J. Ye and S. Liu, *Macromolecules*, 2007, **40**, 9103–9110.
- 232 C. K. Han and Y. H. Bae, *Polymer*, 1998, **39**, 2809–2814.
- 233 A. Durand and D. Hourdet, *Polymer*, 1999, **40**, 4941–4951.
- 234 H.-H. Lin and Y.-L. Cheng, *Macromolecules*, 2001, **34**, 3710–3715.
- 235 C. Li, J. Madsen, S. P. Armes and A. L. Lewis, *Angew. Chem., Int. Ed.*, 2006, **45**, 3510–3513.
- 236 S. E. Kirkland, R. M. Hensarling, S. D. McConaughy, Y. Guo, W. L. Jarrett and C. L. McCormick, *Biomacromolecules*, 2008, **9**, 481–486.
- 237 J. Li, S. Mizutani, S.-i. Sato, A. Narumi, O. Haba, S. Kawaguchi, M. Kikuchi, T. Kakuchi and X. Shen, *Polym. Chem.*, 2020, **11**, 2346–2359.
- 238 R. Watanabe, K. Takaseki, M. Katsumata, D. Matsushita, D. Ida and M. Osa, *Polym. J.*, 2016, **48**, 621–628.
- 239 J. Li, S. Mizutani, S.-i. Sato, A. Narumi, O. Haba, S. Kawaguchi, T. Kakuchi and X. Shen, *Polymer*, 2020, **202**, 122678.
- 240 P. Liu, H. Xie, H. Tang, G. Zhong and H. Zhang, *J. Polym. Sci., Part A: Polym. Chem.*, 2012, **50**, 3664–3673.
- 241 M. A. Ward and T. K. Georgiou, *Soft Matter*, 2012, **8**, 2737–2745.
- 242 J. Li, S. Kikuchi, S.-i. Sato, Y. Chen, L. Xu, B. Song, Q. Duan, Y. Wang, T. Kakuchi and X. Shen, *Macromolecules*, 2019, **52**, 7207–7217.
- 243 B. Jiang, L. Zhang, J. Yan, Q. Huang, B. Liao and H. Pang, *J. Polym. Sci., Part A: Polym. Chem.*, 2014, **52**, 2442–2453.
- 244 H. Yim, M. S. Kent, S. Mendez, G. P. Lopez, S. Satija and Y. Seo, *Macromolecules*, 2006, **39**, 3420–3426.
- 245 K. N. Plunkett, X. Zhu, J. S. Moore and D. E. Leckband, *Langmuir*, 2006, **22**, 4259–4266.
- 246 S. Kunugi, K. Takano, N. Tanaka, K. Suwa and M. Akashi, *Macromolecules*, 1997, **30**, 4499–4501.
- 247 J. P. Magnusson, A. Khan, G. Pasparakis, A. O. Saeed, W. Wang and C. Alexander, *J. Am. Chem. Soc.*, 2008, **130**, 10852–10853.
- 248 X. Liu, F. Cheng, H. Liu and Y. Chen, *Soft Matter*, 2008, **4**, 1991–1994.
- 249 X.-Y. Liu, X.-R. Mu, Y. Liu, H.-J. Liu, Y. Chen, F. Cheng and S.-C. Jiang, *Langmuir*, 2012, **28**, 4867–4876.
- 250 T. J. Murdoch, B. A. Humphreys, E. C. Johnson, G. B. Webber and E. J. Wanless, *J. Colloid Interface Sci.*, 2018, **526**, 429–450.
- 251 Ł. Otulakowski, M. Kasprów, A. Strzelecka, A. Dworak and B. Trzebicka, *Polymers*, 2021, **13**, 90.
- 252 X. Zhao, O. Coutelier, H. H. Nguyen, C. Delmas, M. Destarac and J.-D. Marty, *Polym. Chem.*, 2015, **6**, 5233–5243.
- 253 C. Boutris, E. G. Chatzi and C. Kiparissides, *Polymer*, 1997, **38**, 2567–2570.
- 254 X. Chang, H. Mao, G. Shan, Y. Bao and P. Pan, *ACS Macro Lett.*, 2019, **8**, 357–362.
- 255 L. Liu, W. Li, J. Yan and A. Zhang, *J. Polym. Sci., Part A: Polym. Chem.*, 2014, **52**, 1706–1713.
- 256 A. Li, J. Liu, G. Liu, J. Zhang and S. Feng, *J. Polym. Sci., Part A: Polym. Chem.*, 2014, **52**, 87–95.
- 257 M. Luzon, C. Boyer, C. Peinado, T. Corrales, M. Whittaker, L. Tao and T. P. Davis, *J. Polym. Sci., Part A: Polym. Chem.*, 2010, **48**, 2783–2792.
- 258 K. Rahimian-Bajgiran, N. Chan, Q. Zhang, S. M. Noh, H.-i. Lee and J. K. Oh, *Chem. Commun.*, 2013, **49**, 807–809.
- 259 D. Lipowska-Kur, R. Szweda, B. Trzebicka and A. Dworak, *Eur. Polym. J.*, 2018, **109**, 391–401.
- 260 N. P. Truong, J. F. Quinn, A. Anastasaki, M. Rolland, M. N. Vu, D. M. Haddleton, M. R. Whittaker and T. P. Davis, *Polym. Chem.*, 2017, **8**, 1353–1363.
- 261 W. L. A. Brooks, G. Vancoillie, C. P. Kabb, R. Hoogenboom and B. S. Sumerlin, *J. Polym. Sci., Part A: Polym. Chem.*, 2017, **55**, 2309–2317.
- 262 N. P. Truong, M. R. Whittaker, A. Anastasaki, D. M. Haddleton, J. F. Quinn and T. P. Davis, *Polym. Chem.*, 2016, **7**, 430–440.
- 263 N. T. D. Tran, Z. Jia, N. P. Truong, M. A. Cooper and M. J. Monteiro, *Biomacromolecules*, 2013, **14**, 3463–3471.
- 264 K. Kolouchová, V. Lobaz, H. Beneš, V. R. de la Rosa, D. Babuka, P. Švec, P. Černoch, M. Hrubý, R. Hoogenboom, P. Štěpánek and O. Grobörz, *Polym. Chem.*, 2021, **12**, 5077–5084.
- 265 E. Read, B. Lonetti, S. Gineste, A. T. Sutton, E. Di Cola, P. Castignolles, M. Gaborieau, A. F. Mingotaud, M. Destarac and J. D. Marty, *J. Colloid Interface Sci.*, 2021, **590**, 268–276.
- 266 J. Lyngsø, N. Al-Manasir, M. A. Behrens, K. Zhu, A.-L. Kjøniksen, B. Nyström and J. S. Pedersen, *Macromolecules*, 2015, **48**, 2235–2243.
- 267 J. Korpanty, L. R. Parent, N. Hampu, S. Weigand and N. C. Gianneschi, *Nat. Commun.*, 2021, **12**, 6568.
- 268 B. Wang, T. Xiao, X.-B. Fu, T.-T. Jiang, Y. Chen and Y.-F. Yao, *Macromolecules*, 2017, **50**, 9647–9655.



- 269 C. Zhang, H. Peng, W. Li, L. Liu, S. Puttick, J. Reid, S. Bernardi, D. J. Searles, A. Zhang and A. K. Whittaker, *Macromolecules*, 2016, **49**, 900–908.
- 270 X. Laloyaux, B. Mathy, B. Nysten and A. M. Jonas, *Langmuir*, 2010, **26**, 838–847.
- 271 L. Li, Y. Zhu, B. Li and C. Gao, *Langmuir*, 2008, **24**, 13632–13639.
- 272 V. P. Gilcreest, W. M. Carroll, Y. A. Rochev, I. Blute, K. A. Dawson and A. V. Gorelov, *Langmuir*, 2004, **20**, 10138–10145.
- 273 H. Robertson, E. C. Johnson, I. J. Gresham, S. W. Prescott, A. Nelson, E. J. Wanless and G. B. Webber, *J. Colloid Interface Sci.*, 2021, **586**, 292–304.
- 274 D. Schmaljohann, M. Nitschke, R. Schulze, A. Eing, C. Werner and K.-J. Eichhorn, *Langmuir*, 2005, **21**, 2317–2322.
- 275 A. Sivokhin, D. Orekhov, O. Kazantsev, O. Sivokhina, S. Orekhov, D. Kamorin, K. Otopkova, M. Smirnov and R. Karpov, *Polymers*, 2022, **14**, 137.
- 276 L. Ma, G. Wang, S. Sun and P. Wu, *Phys. Chem. Chem. Phys.*, 2017, **19**, 22263–22271.
- 277 F. Käfer, M. Pretschner and S. Agarwal, *Macromol. Rapid Commun.*, 2018, **39**, 1800640.
- 278 F. Käfer, A. Lerch and S. Agarwal, *J. Polym. Sci., Part A: Polym. Chem.*, 2017, **55**, 274–279.
- 279 A. Espinha, M. C. Serrano, Á. Blanco and C. López, *Adv. Opt. Mater.*, 2014, **2**, 516–521.
- 280 J. Akimoto, Y. Ito, T. Okano and M. Nakayama, *J. Polym. Sci., Part A: Polym. Chem.*, 2018, **56**, 1695–1704.
- 281 S. Arias, F. Freire, M. Calderón and J. Bergueiro, *Angew. Chem., Int. Ed.*, 2017, **56**, 11420–11425.
- 282 L. Xiang, X. Liu, H. Zhang, N. Zhao and K. Zhang, *Polym. Chem.*, 2020, **11**, 6157–6162.
- 283 Kiran, R. Koyilapu, R. Tiwari, S. Krishnamoorthi and K. Kumar, *Global Chall.*, 2020, **4**, 1900089.
- 284 A. Rank, S. Hauschild, S. Förster and R. Schubert, *Langmuir*, 2009, **25**, 1337–1344.
- 285 N. Oleszko, W. Wałach, A. Utrata-Wesołek, A. Kowalczyk, B. Trzebicka, A. Kłama-Baryła, D. Hoff-Lenczewska, M. Kawecki, M. Lesiak, A. L. Sieroń and A. Dworak, *Biomacromolecules*, 2015, **16**, 2805–2813.
- 286 D. Healy, M. E. Nash, A. Gorelov, K. Thompson, P. Dockery, S. Beloshapkin and Y. Rochev, *Macromol. Biosci.*, 2017, **17**, 1600175.
- 287 S. A. Jadhav, I. Miletto, V. Brunella, G. Berlier and D. Scalarone, *Polym. Adv. Technol.*, 2015, **26**, 1070–1075.
- 288 M. A. da Silva, P. Haddow, S. B. Kirton, W. J. McAuley, L. Porcar, C. A. Dreiss and M. T. Cook, *Adv. Funct. Mater.*, 2022, **32**, 2109010.
- 289 Z. Li, Z. Zhang, K. L. Liu, X. Ni and J. Li, *Biomacromolecules*, 2012, **13**, 3977–3989.
- 290 J. Bassi da Silva, P. Haddow, M. L. Bruschi and M. T. Cook, *J. Mol. Liq.*, 2022, **346**, 117906.
- 291 Z. Osváth and B. Iván, *Macromol. Chem. Phys.*, 2017, **218**, 1600470.
- 292 Q. Li, A. P. Constantinou and T. K. Georgiou, *J. Polym. Sci.*, 2021, **59**, 230–239.
- 293 C. M. Jeffries, J. Ilavsky, A. Martel, S. Hinrichs, A. Meyer, J. S. Pedersen, A. V. Sokolova and D. I. Svergun, *Nat. Rev. Methods Primers*, 2021, **1**, 70.
- 294 P. S. Singh, in *Membrane Characterization*, ed. N. Hilal, A. F. Ismail, T. Matsuura and D. Oatley-Radcliffe, Elsevier, 2017, pp. 95–111. DOI: [10.1016/B978-0-444-63776-5.00006-1](https://doi.org/10.1016/B978-0-444-63776-5.00006-1).
- 295 S. Wellert, A. Radulescu, A. Carl, R. von Klitzing and K. Gawlitza, *Macromolecules*, 2015, **48**, 4901–4909.
- 296 K. Nishi, T. Hiroi, K. Hashimoto, K. Fujii, Y.-S. Han, T.-H. Kim, Y. Katsumoto and M. Shibayama, *Macromolecules*, 2013, **46**, 6225–6232.
- 297 A. Papagiannopoulos, J. Zhao, G. Zhang, S. Pispas and A. Radulescu, *Eur. Polym. J.*, 2014, **56**, 59–68.
- 298 S. Salzinger, S. Huber, S. Jaksch, P. Busch, R. Jordan and C. M. Papadakis, *Colloid Polym. Sci.*, 2012, **290**, 385–400.
- 299 S. Jaksch, A. Schulz, K. Kyriakos, J. Zhang, I. Grillo, V. Pipich, R. Jordan and C. M. Papadakis, *Colloid Polym. Sci.*, 2014, **292**, 2413–2425.
- 300 I. Krakovský, L. Hanyková, G. Paladini and L. Almásy, *Eur. Polym. J.*, 2020, **137**, 109929.
- 301 Q. Zhang, J.-D. Hong and R. Hoogenboom, *Polym. Chem.*, 2013, **4**, 4322–4325.
- 302 M. Sahn, T. Yildirim, M. Dirauf, C. Weber, P. Sungur, S. Hoeppeener and U. S. Schubert, *Macromolecules*, 2016, **49**, 7257–7267.
- 303 B. Yu, A. B. Lowe and K. Ishihara, *Biomacromolecules*, 2009, **10**, 950–958.
- 304 S. Jiang, Y. Yao, Q. Chen and Y. Chen, *Macromolecules*, 2013, **46**, 9688–9697.
- 305 C. Xue, N. Yonet-Tanyeri, N. Brouette, M. Sferrazza, P. V. Braun and D. E. Leckband, *Langmuir*, 2011, **27**, 8810–8818.
- 306 Y. Zou, N. A. A. Rossi, J. N. Kizhakkedathu and D. E. Brooks, *Macromolecules*, 2009, **42**, 4817–4828.
- 307 Y. Stetsyshyn, J. Raczowska, O. Lishchynskyi, A. Bernasik, A. Kostruba, K. Harhay, H. Ohar, M. M. Marzec and A. Budkowski, *ACS Appl. Mater. Interfaces*, 2017, **9**, 12035–12045.
- 308 J. I. Kim, B. S. Lee, C. Chun, J.-K. Cho, S.-Y. Kim and S.-C. Song, *Biomaterials*, 2012, **33**, 2251–2259.
- 309 P. Wang, J. He, P.-N. Wang and J.-Y. Chen, *Photomed. Laser Surg.*, 2010, **28**, 201–205.
- 310 E. E. Antunez, C. S. Mahon, Z. Tong, N. H. Voelcker and M. Müllner, *Biomacromolecules*, 2021, **22**, 441–453.
- 311 T. Elshaarani, H. Yu, L. Wang, R. S. Ullah, S. Fahad, K. Ur Rahman, A. Khan, A. Nazir, M. Usman, R. U. Khan, F. Haq, R. Liang, X. Chen and M. Haroon, *J. Mater. Sci.*, 2019, **54**, 10009–10023.
- 312 Q. Mao, K. Liu, W. Li, J. Yan and A. Zhang, *Polym. Chem.*, 2015, **6**, 1300–1308.
- 313 A. D'Emanuele and R. Dinarvand, *Int. J. Pharm.*, 1995, **118**, 237–242.
- 314 S. K. Li and A. D'Emanuele, *J. Controlled Release*, 2001, **75**, 55–67.
- 315 X.-Z. Zhang, R.-X. Zhuo, J.-Z. Cui and J.-T. Zhang, *Int. J. Pharm.*, 2002, **235**, 43–50.



- 316 S. Ilić-Stojanović, L. Nikolić, V. Nikolić, I. Ristić, S. Cakić and S. D. Petrović, *Gels*, 2023, **9**, 70.
- 317 R. Dinarvand and A. D'Emanuele, *J. Controlled Release*, 1995, **36**, 221–227.
- 318 S. Nayak, D. Gan, M. J. Serpe and L. A. Lyon, *Small*, 2005, **1**, 416–421.
- 319 J. Akimoto, M. Nakayama, K. Sakai and T. Okano, *Biomacromolecules*, 2009, **10**, 1331–1336.
- 320 Q. Zhang, Z. Hou, B. Louage, D. Zhou, N. Vanparijs, B. G. De Geest and R. Hoogenboom, *Angew. Chem., Int. Ed.*, 2015, **54**, 10879–10883.
- 321 M. Hruby, C. Konak, J. Kucka, M. Vetrik, S. K. Filippov, D. Vetvicka, H. Mackova, G. Karlsson, K. Edwards, B. Rihova and K. Ulbrich, *Macromol. Biosci.*, 2009, **9**, 1016–1027.
- 322 Z. Li, S. Cho, I. C. Kwon, M. M. Janát-Amsbury and K. M. Huh, *Carbohydr. Polym.*, 2013, **92**, 2267–2275.
- 323 Retrieved from <https://clinicaltrials.gov/>, search term: Genexol-PM, accessed in July, 2023.
- 324 M. Karayilan, L. Clamen and M. L. Becker, *Biomacromolecules*, 2021, **22**, 223–261.
- 325 E. C. Abenojar, S. Wickramasinghe, M. Ju, S. Uppaluri, A. Klika, J. George, W. Barsoum, S. J. Frangiamore, C. A. Higuera-Rueda and A. C. S. Samia, *ACS Infect. Dis.*, 2018, **4**, 1246–1256.
- 326 S. Wickramasinghe, M. Ju, N. B. Milbrandt, Y. H. Tsai, M. Navarreto-Lugo, A. Visperas, A. Klika, W. Barsoum, C. A. Higuera-Rueda and A. C. S. Samia, *ACS Appl. Nano Mater.*, 2020, **3**, 5862–5873.
- 327 N. B. Milbrandt, Y. H. Tsai, K. Cui, C. S. Ngompe Massado, H. Jung, A. Visperas, A. Klika, N. Piuze, C. A. Higuera-Rueda and A. C. S. Samia, *ACS Appl. Bio Mater.*, 2023, **6**, 1231–1241.
- 328 N. Bhattarai, J. Gunn and M. Zhang, *Adv. Drug Delivery Rev.*, 2010, **62**, 83–99.
- 329 L. H. Lima, Y. Morales and T. Cabral, *J. Ophthalmol.*, 2016, **2016**, 5356371.
- 330 N. Bayat, Y. Zhang, P. Falabella, R. Menefee, J. J. Whalen, M. S. Humayun and M. E. Thompson, *Sci. Transl. Med.*, 2017, **9**, eaan3879.
- 331 G.-H. Hsiue, S.-h. Hsu, C.-C. Yang, S.-H. Lee and I. K. Yang, *Biomaterials*, 2002, **23**, 457–462.
- 332 F. S. Mah, *J. Ocul. Pharmacol. Ther.*, 2016, **32**, 396–399.
- 333 H. Cho, J. Gao and G. S. Kwon, *J. Controlled Release*, 2016, **240**, 191–201.
- 334 N. L. Elstad and K. D. Fowers, *Adv. Drug Delivery Rev.*, 2009, **61**, 785–794.
- 335 S. Tanga, M. Aucamp and P. Ramburrun, *Gels*, 2023, **9**, 418.
- 336 A. P. Constantinou and T. K. Georgiou, *Polym. Int.*, 2021, **70**, 1433–1448.
- 337 M. M. Allyn, R. H. Luo, E. B. Hellwarth and K. E. Swindle-Reilly, *Front. Med.*, 2022, **8**, 1–25.
- 338 E. Behraves and A. G. Mikos, *J. Biomed. Mater. Res., Part A*, 2003, **66A**, 698–706.
- 339 K. Nagase, J. Kobayashi, A. Kikuchi, Y. Akiyama, H. Kanazawa and T. Okano, *Langmuir*, 2007, **23**, 9409–9415.
- 340 K. Nagase, J. Kobayashi and T. Okano, *J. R. Soc., Interface*, 2009, **6**, S293–S309.
- 341 K. Nagase, M. Watanabe, A. Kikuchi, M. Yamato and T. Okano, *Macromol. Biosci.*, 2011, **11**, 400–409.
- 342 K. Nagase and T. Okano, *J. Mater. Chem. B*, 2016, **4**, 6381–6397.
- 343 K. Nagase and T. Okano, *Polymer and Biopolymer Brushes*, 2017, pp. 361–375. DOI: [10.1002/9781119455042.ch12](https://doi.org/10.1002/9781119455042.ch12).
- 344 H. Kanazawa, K. Yamamoto, Y. Matsushima, N. Takai, A. Kikuchi, Y. Sakurai and T. Okano, *Anal. Chem.*, 1996, **68**, 100–105.
- 345 S. Radtke, J. E. Adair, M. A. Giese, Y. Y. Chan, Z. K. Norgaard, M. Enstrom, K. G. Haworth, L. E. Scheffer and H. P. Kiem, *Sci. Transl. Med.*, 2017, **9**, 1–22.
- 346 U. A. Gurkan, T. Anand, H. Tas, D. Elkan, A. Akay, H. O. Keles and U. Demirci, *Lab Chip*, 2011, **11**, 3979–3989.
- 347 U. A. Gurkan, S. Tasoglu, D. Akkaynak, O. Avci, S. Unluisler, S. Canikyan, N. MacCallum and U. Demirci, *Adv. Healthcare Mater.*, 2012, **1**, 661–668.
- 348 H. A. von Recum, S. W. Kim, A. Kikuchi, M. Okuhara, Y. Sakurai and T. Okano, *J. Biomed. Mater. Res.*, 1998, **40**, 631–639.
- 349 H.-W. Kang, Y. Tabata and Y. Ikada, *Biomaterials*, 1999, **20**, 1339–1344.
- 350 H. Shin, P. Quinten Ruhé, A. G. Mikos and J. A. Jansen, *Biomaterials*, 2003, **24**, 3201–3211.
- 351 T. Sun and G. Qing, *Adv. Mater.*, 2011, **23**, H57–H77.
- 352 R. Suntornnond, J. An and C. K. Chua, *Macromol. Mater. Eng.*, 2017, **302**, 1600266.
- 353 I. K. Kwon and T. Matsuda, *Biomaterials*, 2006, **27**, 986–995.
- 354 J. Zhong, H. Wang, K. Yang, H. Wang, C. Duan, N. Ni, L. An, Y. Luo, P. Zhao, Y. Gou, S. Sheng, D. Shi, C. Chen, W. Wagstaff, B. Hendren-Santiago, R. C. Haydon, H. H. Luu, R. R. Reid, S. H. Ho, G. A. Ameer, L. Shen, T.-C. He and J. Fan, *Bioact. Mater.*, 2022, **9**, 523–540.
- 355 M. D. Pawar, G. V. N. Rathna, S. Agrawal and B. S. Kuchekar, *Mater. Sci. Eng., C*, 2015, **48**, 126–137.
- 356 Q. X. Ji, J. Deng, X. M. Xing, C. Q. Yuan, X. B. Yu, Q. C. Xu and J. Yue, *Carbohydr. Polym.*, 2010, **82**, 1153–1160.
- 357 I. Ishikawa, T. Iwata, K. Washio, T. Okano, T. Nagasawa, K. Iwasaki and T. Ando, *Periodontol. 2000*, 2009, **51**, 220–238.
- 358 T. Iwata, M. Yamato, H. Tsuchioka, R. Takagi, S. Mukobata, K. Washio, T. Okano and I. Ishikawa, *Biomaterials*, 2009, **30**, 2716–2723.
- 359 K. Washio, T. Iwata, M. Mizutani, T. Ando, M. Yamato, T. Okano and I. Ishikawa, *Cell Tissue Res.*, 2010, **341**, 397–404.
- 360 K. Nishida, M. Yamato, Y. Hayashida, K. Watanabe, N. Maeda, H. Watanabe, K. Yamamoto, S. Nagai,



- A. Kikuchi, Y. Tano and T. Okano, *Transplantation*, 2004, **77**, 379–385.
- 361 K. Nishida, M. Yamato, Y. Hayashida, K. Watanabe, K. Yamamoto, E. Adachi, S. Nagai, A. Kikuchi, N. Maeda, H. Watanabe, T. Okano and Y. Tano, *N. Engl. J. Med.*, 2004, **351**, 1187–1196.
- 362 T. Ide, K. Nishida, M. Yamato, T. Sumide, M. Utsumi, T. Nozaki, A. Kikuchi, T. Okano and Y. Tano, *Biomaterials*, 2006, **27**, 607–614.
- 363 M. Khalili, A. Zarebkohan, H. Dianat-Moghadam, M. Panahi, H. Andre and E. Alizadeh, *Chem. Eng. J.*, 2022, **429**, 132523.

